ARMY RESEARCH LABORATORY

AR

Micromechanical Measurement System for Thin Films on Polymeric Substrates

Wayne Bonin and Jerzy T. Wyrobek

ARL-CR-180   March 1995

19950803 028

DISCLAIMER NOTICE

THIS DOCUMENT IS BEST QUALITY AVAILABLE. THE COPY FURNISHED TO DTIC CONTAINED A SIGNIFICANT NUMBER OF PAGES WHICH DO NOT REPRODUCE LEGIBLY.

REPORT DOCUMENTATION PAGE

Public reporting burden for this collection of information is estimated to average 1 hour per response, including the time for reviewing instructions, searching existing data sources, gathering and maintaining the data needed, and completing and reviewing the collection of information. Send comments regarding this burden estimate or any other aspect of this collection of information, including suggestions for reducing this burden, to Washington Headquarters Services, Directorate for Information Operations and Reports, 1215 Jefferson Davis Highway, Suite 1204, Arlington, VA 22202-4302, and to the Office of Management and Budget, Paperwork Reduction Project (0704-0188), Washington, DC 20503.

1. AGENCY USE ONLY *(Leave blank)*	2. REPORT DATE March 1995	3. REPORT TYPE AND DATES COVERED Final 3/10/94 - 9/9/94

4. TITLE AND SUBTITLE Micromechanical Measurement System for Thin Films on Polymeric Substrates	5. FUNDING NUMBERS DAAL01-94-C-4024
6. AUTHOR(S) Wayne Bonin and Jerzy T. Wyrobek	

7. PERFORMING ORGANIZATION NAME(S) AND ADDRESS(ES) Hysitron Incorporated 2010 E. Hennepin Ave. Minneapolis, MN 55413	8. PERFORMING ORGANIZATION REPORT NUMBER

9. SPONSORING/MONITORING AGENCY NAME(S) AND ADDRESS(ES) Army Research Laboratory Watertown, MA 02172-0001 ATTN: AMSRL-MA-PB	10. SPONSORING/MONITORING AGENCY REPORT NUMBER ARL-CR-180

11. SUPPLEMENTARY NOTES

COR: Alex Hsieh

12a. DISTRIBUTION/AVAILABILITY STATEMENT Approved for public release; distribution unlimited.	12b. DISTRIBUTION CODE

13. ABSTRACT *(Maximum 200 words)*

14. SUBJECT TERMS Microindentation, Microscratch, Diamond-like Carbon (DLC), Thin Films	15. NUMBER OF PAGES 37
	16. PRICE CODE

17. SECURITY CLASSIFICATION OF REPORT Unclassified	18. SECURITY CLASSIFICATION OF THIS PAGE Unclassified	19. SECURITY CLASSIFICATION OF ABSTRACT Unclassified	20. LIMITATION OF ABSTRACT UL

NSN 7540-01-280-5500

Micromechanical Measurement System
for
Thin Films on Polymeric Substrates

In Situ

Final Technical Report
Phase 1

HYSITRON INC.
December 21ST, 1994

<u>Title:</u>   Micromechanical Measurement System for Thin Films on Polymeric Substrates, Results of Phase I Work (Final Report)

<u>Name of Contractor:</u>   Hysitron Incorporated
2010 E Hennepin Ave
Minneapolis, MN 55413
Attn: Jerzy T. Wyrobek   612-722-5358

Accesion For	
NTIS CRA&I	☑
DTIC TAB	☐
Unannounced	☐
Justification	
By	
Distribution /	
Availability Codes	
Dist	Avail and/or Special
A-1	

<u>Contract Number:</u>   DAAL01-94-C-4024

<u>Key Person:</u>   Wayne Bonin   612-379-4179

<u>Reporting Period:</u>   March 10, 1994   through   September 9, 1994

<u>Report prepared by:</u>

Wayne Bonin (signature)

Wayne Bonin
612-379-4179
612-379-0678 fax

<u>Approved by:</u>

Jerzy T. Wyrobek (signature)

Jerzy T. Wyrobek, Pres. Hysitron
612-722-5358
fax 612-722-0493

1

Summary of Results

The overall objective of the Phase I project was to demonstrate the feasibility of building an instrument that would provide the combined capability of micromechanical testing and high resolution *in situ* imaging in a single instrument. The exact region of a sample could then be inspected and images recorded immediately before and after indenting or scratching without having to reposition the sample. The specific application of the instrument of interest to the Army was testing mechanical properties such as adhesion, scratch resistance and fracture resistance of very thin (in the range of 0.1µm) hard films such as DLC on polymeric substrates such as polycarbonate. It was also anticipated that developing such an instrument, suitable for testing the described hard films, would be useful as a microhardness/micromechanical test system for general purpose laboratory use with a wide range of materials of both commercial and theoretical interest.

As proposed, feasibility of the concept has been demonstrated by building a prototype system using our capacitive force/displacement sensor to measure the force applied to the sample, with the required scanning and indenting motion applied by a commercial STM piezo, and imaging provided by the same commercial STM system. Results of the Phase I effort have been quite successful. AFM imaging has been developed as planned, so that both conductive and non-conductive materials can be imaged by the system, and also allowing undoped, non-conductive diamond tips to be used. The minimum force level we have been able to operate at during imaging is about 0.5µN, with 1µN being more reliable for longer periods of time. It was found that no damage to a GaAs surface occurred at an imaging force of 1µN, although 2.5µN did cause damage. Hard coatings can be easily imaged in AFM mode without damage, as demonstrated by the finding that 1000Å DLC films required 29µN to damage the surface.

Loads up to 2.5mN (250mg) can be applied, with a resolution of 0.1µN (0.01mg). Lateral resolution of 10nm and vertical resolution of 1nm has been demonstrated. The present load capacity will allow the instrument to test DLC films significantly thicker than the 0.1µm value specified in the original solicitation. It is expected to be useful for films up to at least 1µm thickness for DLC and greater for other materials of lesser strength.

Detailed results

Equipment: The equipment used to demonstrate the feasibility of the micromechanical test system with *in situ* STM/AFM imaging consists of a Hysitron capacitive force/displacement transducer used in conjunction with a commercial scanning tunneling microscope (STM). We used a Digital Instruments, Inc. Nanoscope III STM, renting time on it from the Center for Interfacial Engineering (CIE) at the University of Minnesota.

A block diagram of the STM/AFM force sensor system is shown in **Figure 1.** The three boxes labeled NANOSCOPE III STM CONTROLLER, VIDEO DISPLAY MONITOR and 3-D PIEZO ACTUATOR are from the Digital Instruments Nanoscope III STM, which we are renting time on. The rest of the equipment was built by Hysitron.
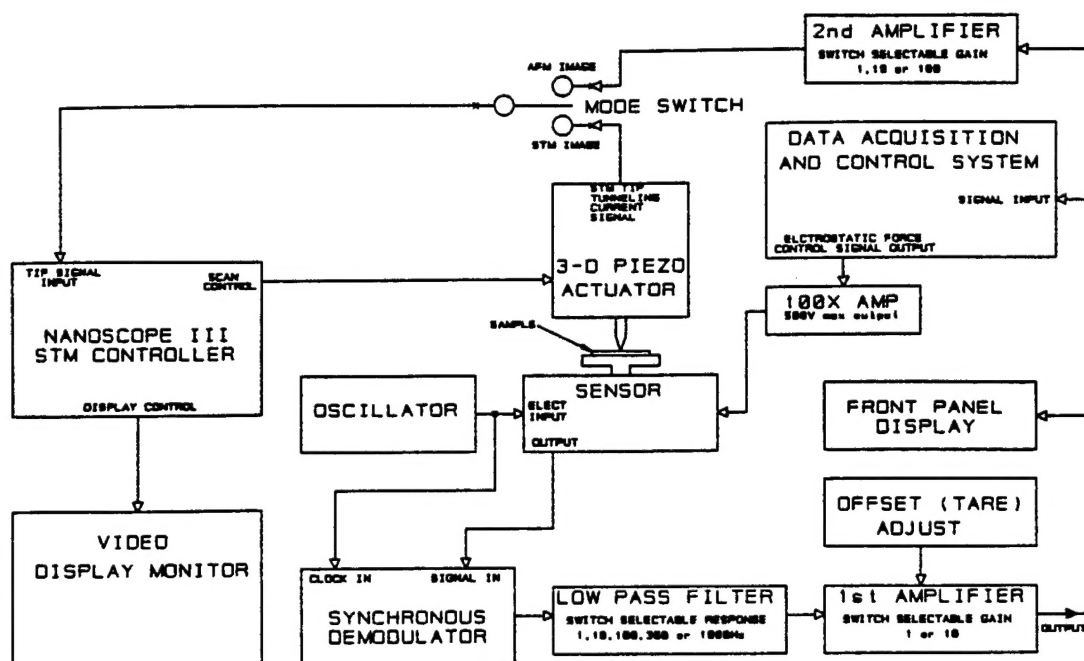

Figure 1. Diagram of STM/AFM force sensor system.

The blocks labeled OSCILLATOR, SYNCHRONOUS DEMODULATOR, and 100X AMP (with 500V output) are located on a $3\frac{1}{2}$ inch diameter circuit board that mounts on the STM base. The sensor is mounted on the STM base as well, in a cut out in the center of the circuit board. The sensor is connected to the circuit board by a flexible cable terminated in an 8 pin DIP socket. The sensor is held to the STM base by three small magnets in the bottom of the sensor, which hold it firmly but allow movement for easy positioning. Samples are held in place on the sensor by small metal spring clips, so they can be easily exchanged.

With the mode switch connected to the STM tip signal ("STM IMAGE" position), the system operates as a normal STM, but with the added capability of monitoring the force between tip and sample during operation, and forces exerted on the sample during testing (indenting or scratching). Imaging is then performed without disturbing sample position. For STM imaging, it is necessary to connect the bias voltage from the STM base to the sample with a fine wire, because the sample is no longer sitting directly on the base.

3

To operate in AFM mode with the STM tip, the mode switch is set to "AFM IMAGE", connecting the force signal output from the force sensor to the tip signal input of the STM controller. In this mode, the system images by maintaining a constant force between the tip and the sample. The image signal is the voltage applied to the z-axis piezo, which represents the height (topography) of the sample. This signal is normally scaled and displayed in nanometers.

Since the STM control system has not been modified, the setting menu and image display contain certain items specific to STM operation that have different meaning when operating in AFM mode. The bias voltage setting (used to set the potential between the tip and sample for creating tunneling current) is no longer relevant. It can be set to zero or left at whatever it was. The tunneling current set point (set point) is now used to control the tip to sample force during imaging. Although the set point is displayed as a current, the system actually responds to the voltage output of the current to voltage converter inside the 3-D piezo actuator. This converter has a scale factor of 100mV/nA.

The Hysitron force sensor has been calibrated to a scale factor of 1mV/mg (100mV/mN) for 1st and 2nd amplifiers both set at 1X. Normally the 1st amplifier is set at 10X, which gives a full scale reading of 199.99mg (1.96mN), and the second amplifier is set at 100X. With this combination, the operating force during imaging is 1µN (0.1mg) per nA of the set point.

Imaging is normally done at 1µN of force, but it is usually necessary to set it at 2 to 3 µN when engaging the tip to the sample. Once engaged, the force can be reduced. Engagement sometimes produces transient forces exceeding the set point. If that is a problem, a small region of the sample can be used for engagement, and the tip then moved to a different location after engaging and reducing to the desired operating force, to prevent damage to the test region.

The data acquisition system is normally used to record the output of the sensor during indent or scratch testing of the sample, although it can record the forces present at any time, such as during imaging also. The control section of the data acquisition system is used with electrostatic force application, which will be described following the description of piezo force application.

Forces can be applied to the sample for micromechanical testing in two ways. One of the methods is to drive the tip into the sample using the Z-axis piezo. This can be controlled by writing "lithography scripts" that run under the Digital Instruments Nanoscope III control system. These scripts can be used to control the tip motion in all three axes. Simultaneous motion in Z and X or Y is not supported, so the force ramp desired for continuous microscratch testing has to be approximated using a staircase type ramp. The maximum force that can be applied to the sample in this manner is determined by the Z-axis travel of the piezo and the spring constant of the force sensor. For the 742F piezo scan head and force sensor 3MTS#5, this is a little over 3µm times 99.0µN/µm or 300µN (30mg). This is a rather limited force, but we have been able to do significant testing with it. Higher forces could be achieved by using a sensor with a higher spring constant, but that would decrease the

resolution and increase the required minimum imaging force, possibly causing sample wear problems during imaging. Another limitation with this method of force application is that the Z-axis travel of the piezo actuator is not compensated for linearity and hysteresis effects, as are the X and Y-axis. This results in rather large differences between the commanded Z-axis travel in the lithography script and the actual travel. From the calibrated displacement sensitivity of our sensor of 10.1 mV/μm, we have determined that the Z-axis piezo actually travels slightly over 3μm when commanded to travel 2μm, and travels about 0.7μm when commanded to travel 0.5μm. Although it is possible to calibrate the Z-axis piezo to achieve accuracy of 5 to 10%, hysteresis, non-linearity and time dependencies would make it difficult and time consuming to obtain accuracy better than that.

It was originally planned to obtain the penetration depth of the tip into the sample by subtracting the sample movement on the sensor (sensor force output times spring constant) from the Z-axis motion commanded in the lithography script. Rather than pursue this approach, with its problems as described above, we decided to add electrostatic actuation to the sensor.

With electrostatic actuation, a relatively high voltage (500V maximum) is applied to the upper drive plate of the sensor. The electrostatic attraction between the spring mounted center electrode and the fixed upper drive plate pulls the center electrode up, driving the sample into the tip. The force is determined by the applied voltage and center electrode to drive plate spacing. This spacing can be determined from the output signal of the sensor, which is now used to represent position rather than force. With the present sensor, the maximum force is about 2.5mN (250mg) at 500V. This varies somewhat with sample weight, as heavier samples increase the center electrode to top drive plate spacing, and the force is proportional to the square of the electric field. A maximum force of 2.5mN seems adequate for a practical test instrument, but it may be possible to increase this force significantly by reducing the plate spacing, using different thickness spacers in the sensor assembly.

Indents are performed by setting the scan size to zero. This procedure stops the tip from scanning while leaving it in contact with the surface. The feedback gains are also set to zero to prevent the STM control system from moving the Z-axis piezo in response to changes in the sensor output during indenting. The sensor output represents the sample position. Since the tip position is relatively rigid compared to the penetration of the tip into the sample, the tip can normally be assumed to be fixed in location, so the sensor output represents the indent depth directly. Load/displacement curves are obtained by plotting the force (as determined by the applied voltage) versus the penetration depth obtained from the sensor. The force is presently determined manually from calibration curves. (Automating the conversion task and including it in the data acquisition and control system is a straight forward task, but there was not enough time to do it during Phase I as electrostatic actuation was not originally intended to be part of the Phase I work.)

The 500V power supply and amplifier are located on the 3½ inch circuit board mounted on the STM base. The maximum output current of the 500V supply is only about 2mA, so it is safe even if accidental contact were made with it.

5

<u>Test Results:</u>   While performing initial AFM imaging on DLC films, it was observed that both air currents and vibrations from the building were each contributing 5µN of noise to the signal, by mechanically disturbing the sensor and sample. Attempts to run at less than 5µN resulted in loss of engagement, and approximately 10µN imaging force was required to get relatively noise free images.

The DLC films were prepared for us by Dr. Jack H. Judy at the University of Minnesota. We have samples from three different processes. All of the samples were deposited on 1/16 inch thick Lexan polycarbonate. These images are of the first sample, produced in Dr. Judy's Temescal system. The substrate was etched at 500W RF for 10 minutes at 3mTorr Ar pressure, and coated at 8mTorr Ar pressure at 1.5KW DC, 8 passes at 2mm/second.

<u>Figure 2a and 2b</u> are as received images of the DLC surface. In figure 2a, the imaging force was about 5.7µN (0.58mg). The scratch-like features on the image should be noted. Figure 2b is identical to figure 2a except the operating force was increased to 8.6µN (0.88mg). The scratch-like features in figure 2a are believed to be noise generated by air currents and vibrations from the building, causing forces on the sample in the range of 5µN each, so that somewhat more force needs to be applied to the sample to maintain stable contact. It is possible to image DLC films at loads even higher than this without damage, but other materials are damaged at far lower loads, and scratch tested DLC may have bare polycarbonate regions needing to be imaged also. Hence, lower imaging force was desired.

The vibrations were greatly reduced by placing the scan head on a granite slab suspended from the ceiling by elastic cords, and the air currents were reduced by placing a plexiglass box over the scan head. This has essentially eliminated air currents and vibrations as a limiting factor as to how low the imaging force can be successfully set. Short term signal fluctuations (as would be caused by vibrations and air currents) are about $0.2µN_{p-p}$ with the improvements described. This is an improvement of about 25X.

Another noise source, which affects both the quality of the images and the ability to image at low force, seems to be generated by the Digital Instruments computer system. This noise source produces diagonal lines on the image. This was first noticed with the original amplifier with a single output for the front panel display, data acquisition system and STM controller. The gain could be switched at 1, 10, or 100X. We were able to reduce the effect of the noise by operating our system at a gain of 100, so that the signal was amplified to a higher level before it is subjected to the noise in the computer system.

The problem with this method of noise reduction was that it limited the upper force range that could be measured, due to amplifier saturation, to about 200µN. This limitation was eliminated by providing separate outputs for the data acquisition system and the signal to the STM controller, as shown in the current block diagram, figure 1. This allows the gain to the STM controller to be high (100 or 1000X) to improve the image quality, while the gain to the front panel display and data acquisition system can be low enough to prevent clipping during indenting. <u>Figures 3a, 3b and 3c</u> show the improved image quality (reduction in diagonal noise lines) at higher gains. The indent visible in figures 3a and 3c was the result of re-engaging the tip to get the image
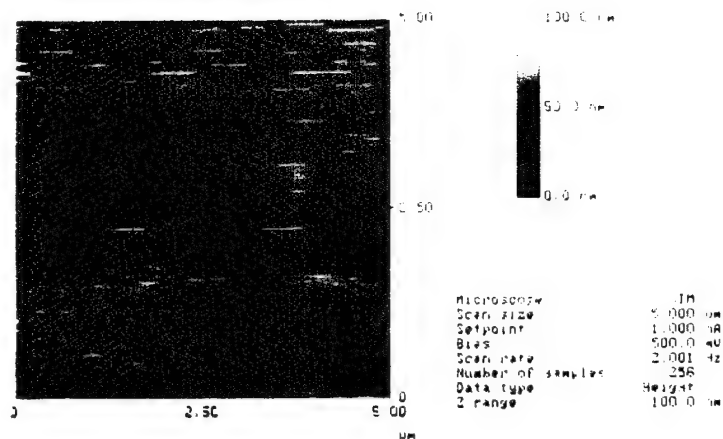
6

100.0 nm

50.0 nm

0.0 nm

Microscope	AFM
Scan size	5.000 µm
Setpoint	1.000 nA
Bias	500.0 mV
Scan rate	2.001 Hz
Number of samples	256
Data type	Height
Z range	100.0 nm

dlc1.001

Figure 2a. DLC sample imaged at 5.7µN. Noisy image due to fluctuations from air currents and vibrations.

100.0 nm

50.0 nm

0.0 nm

Microscope	AFM
Scan size	5.000 µm
Setpoint	1.500 nA
Bias	500.0 mV
Scan rate	2.001 Hz
Number of samples	256
Data type	Height
Z range	100.0 nm

dlc1.002
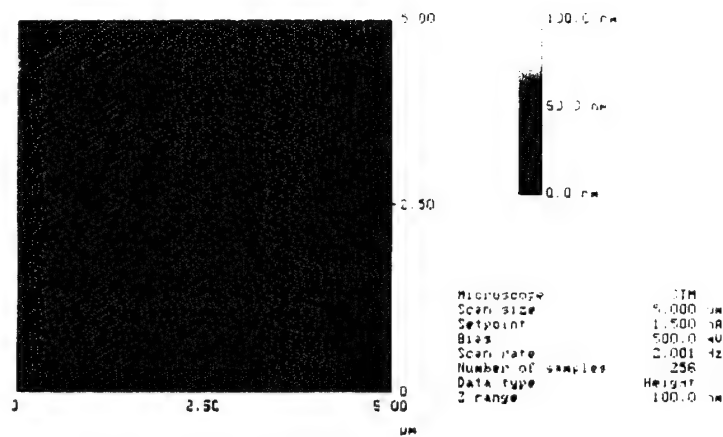
Figure 2b. Same as 2a, except imaged at 8.6µN. Higher force has reduced the noise.

7
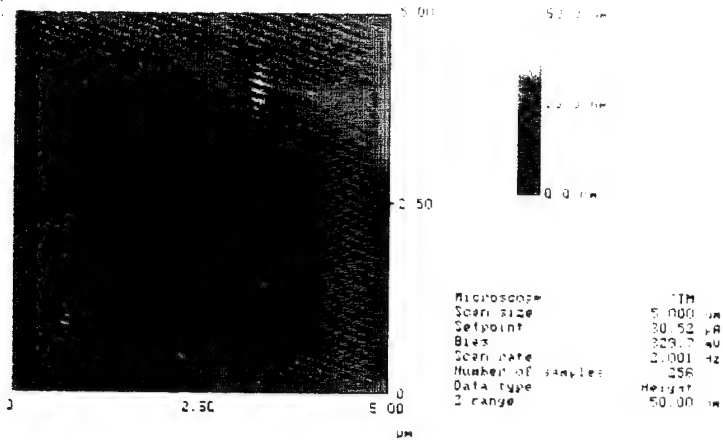
Figure 3a. Polished GaAs wafer surface with total amplifier gain at 10X. Diagonal noise lines are very bad.

gaas7-15.002
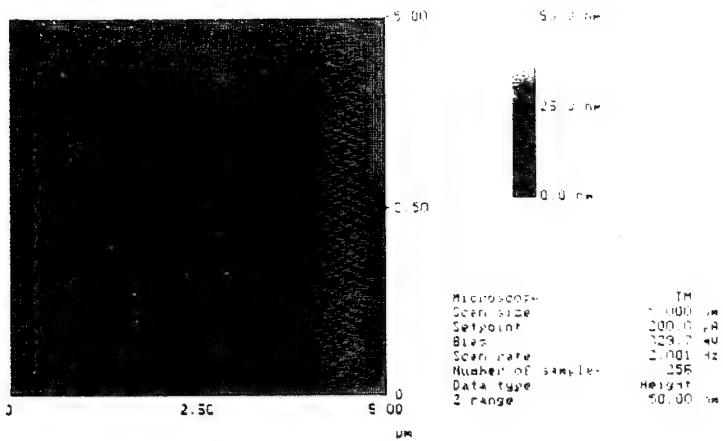
Figure 3b. Same as above, but gain is 100X. Noise is much less.

gaas7-15.001
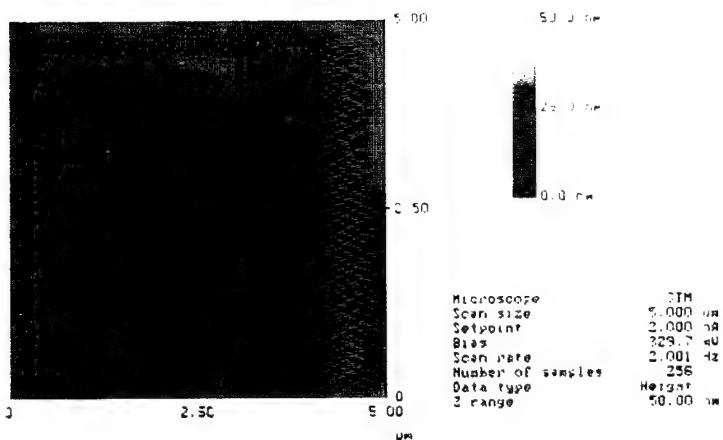
Figure 3c. Same as above, but gain is 1000X. Noise is further reduced.

gaas7-15.003

shown in figure 3a, after the image in figure 3b was scanned (the image in 3b was scanned first, then 3a, followed by 3c).

It was also observed that touching the cable connecting the sensor printed circuit board to the main box containing the amplifiers, filters and power supply caused an output shift of up to 25µN. This problem, which was traced to interference from a switching power supply, was solved by replacing the switching supply with a linear supply. After eliminating the interference, touching the cable had no noticeable effect on the output (less than the 0.1µN resolution of the display).

Further testing showed a second effect caused by touching the base on which the sensor was mounted. The zero level was found to shift by 17µN when the electrically isolated base was touched, and by 27µN when the base was grounded. For normal STM use, the base is connected to the bias voltage supply from the STM controller. Since we do not need this bias voltage for our AFM imaging, we disconnected the bias supply and grounded the base, thus solving this problem.

After making the two changes described above, the system showed much less drift and fluctuation of the zero level. The system now stabilizes to the point of ±0.1µN and the drift rate is less than 0.05µN/minute within five minutes after set up. Previously it took about 30 minutes to reach these levels, if they were achieved at all. Drift rates an low as 0.6µN/hour have been observed after the setup has stabilized for several hours.

With the improvements described above, it is now possible to image at forces as low as 0.5µN (0.05mg). The limiting factor is now drift (probably due to temperature changes). If the drift is in the negative direction, it will increase the operating force and thus the potential to damage the surface. If the drift happens to be in the positive direction and it exceeds the set point, engagement will be lost. Initially it is necessary to withdraw the tip and re-zero the sensor every 5 or 10 minutes, but this time interval can be increased as the unit stabilizes, so that after an hour, it may be necessary to re-zero only once in 15 to 30 minutes.

Wear and surface damage during imaging were studied on surfaces of bare GE LEXAN, 1000Å DLC on LEXAN polycarbonate, and GaAs. The DLC sample could be imaged with no visible damage at 35 times the minimum achievable force. The GaAs sample could be imaged at twice the minimum force with no visible damage, and the bare Lexan could be imaged with acceptably small amounts of damage. These tests were run by imaging a small region, then scanning across it several more times (possibly at a higher force), then imaging a larger region with the original region in the center.

Figure 4a shows a 2µm region of the DLC sample on polycarbonate, imaged during the first scan at a force of 5.8µN (0.59mg). **Figure 4b** shows the same region after five scans, with no visible change other than an image shift that is discussed below. **Figure 4c** shows a 5µm region with the original 2µm region in the center. There is no visible damage to the surface at this force level after five passes. This procedure was repeated at forces of 11.8 and 17.6µN with no visible damage. Damage was finally observed at a scanning force of

9

29μN. **Figure 5a** shows the original 2μm region. The region was then scanned five times at a force of 29μN (3.0mg). The image on the screen during this time showed damage starting with the first scan. **Figure 5b** shows an image of the region after the five scans, with considerable surface damage visible. **Figure 5c** shows an image of a 5μm region with the original region at the center. The dark region in the center is a depression caused by the 29μN scanning force. The section analysis shows the depth of the depression to be 180nm, and to be wedge shaped rather than flat, with material piled up on the right hand side. This is probably due to deformation of the Lexan material under the DLC film, as there does not appear to be any penetration through the DLC.

A comparison of Figures 4a and 4b shows an apparent increase in magnification of figure 4b over 4a in the vertical direction. In particular, the upper 60% of figure 4a seems to have stretched out to fill all of figure 4b. This sort of image shifting is a common complaint with other users of the AFM/STMs at CIE, although no one seems to have been able to resolve the problem. The mechanical support of the STM scan head on the instrument base is the most likely source of the problem.

The Digital Instruments STM scan head is supported on three screws topped by steel balls. The screws are for adjusting the height of the scan head for different sample thicknesses. The scan head sits directly on top of the balls at the end of each screw. Two of the screws are adjusted manually, while the third is set roughly by hand, and then adjusted to the operating setting by a stepper motor under computer control.

The mechanical details of how the scan head sits on the screws was carefully thought out. The two manually adjusted screws fit into a conically tapered hole and a slot, providing a point constraint for one and a line constraint for the other. The third screw is located under a flat part of the scan head, so that the effect of run out of this screw on head position is minimized. The problem is that the screws themselves have slop in the threads, so the potential benefit of the point/line/plane registration system is completely negated.

To remedy this, a base was obtained from Digital Instruments and modified to allow locking of the two manual adjustment screws for more stable images. This was done by drilling and tapping holes perpendicular to the two manual adjustment screws, for set screws to lock the adjustment screws. A small piece of plastic was inserted under the set screws to protect the adjustment screw threads.

Since the instability of the original base was more or less random, and we did not study that effect thoroughly enough to get statistically meaningful results (due to time constraints and priorities) it is difficult to accurately quantify the level of improvement, but it is definitely much better. Figures 4a and 4b show a shift of almost 1μm which occurred during a single scan. Shifts from one scan to the next of up to 0.5μm were common. The new base has eliminated these large shifts. **Figures 6a and 6b** show successive scans of a 500nm region containing a small indent as a visual reference. The tip used for indenting and imaging these figures was Edge Tech #3, with an indent force of 80μN (8.2mg) and an imaging force of 0.9μN (0.09mg). The two scans show
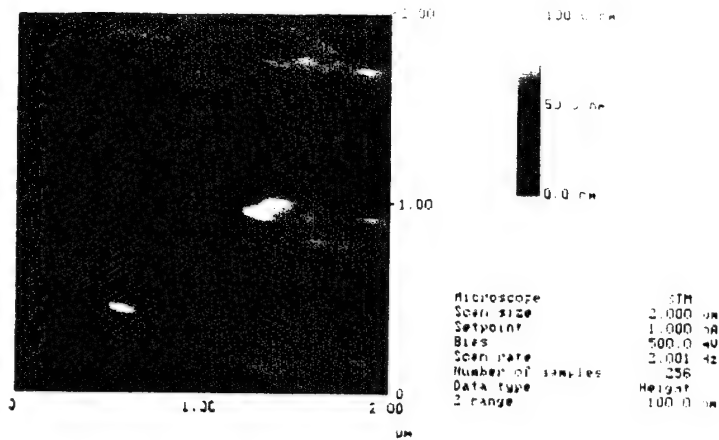
10

Microscope   STM
Scan size   2.000 um
Setpoint   1.000 nA
Bias   500.0 mV
Scan rate   2.001 Hz
Number of samples   256
Data type   Height
Z range   100.0 nm

05101854.001

Figure 4a. DLC sample on first scan at 5.8µN imaging force

Microscope   STM
Scan size   2.000 um
Setpoint   1.000 nA
Bias   500.0 mV
Scan rate   2.001 Hz
Number of samples   256
Data type   Height
Z range   100.0 nm
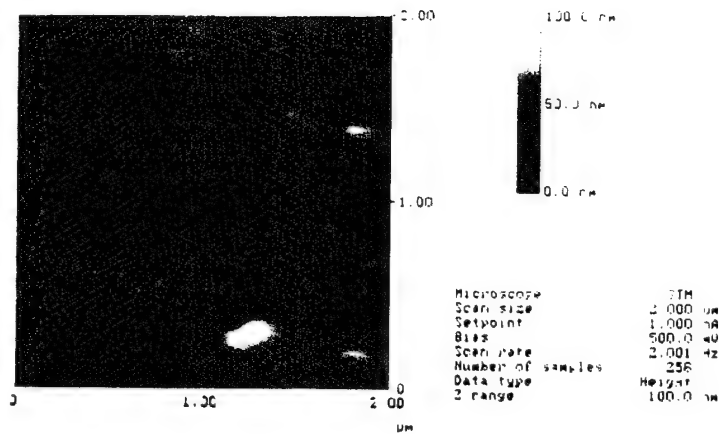
dlc5.000

Figure 4b. DLC sample on fifth scan at 5.8µN imaging force.

Microscope   STM
Scan size   5.000 um
Setpoint   1.000 nA
Bias   500.0 mV
Scan rate   2.001 Hz
Number of samples   256
Data type   Height
Z range   100.0 nm

dlc3.001
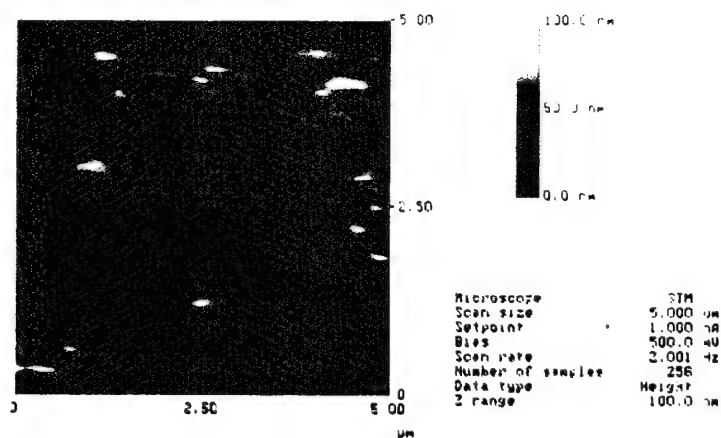
Figure 4c. Scan of larger area, centered around region shown in figure 4b. No surface damage visible at 5.8µN force level.

11
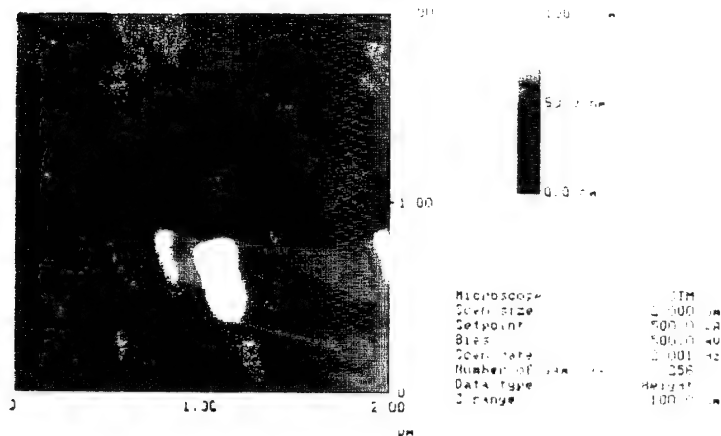
Figure 5a. DLC sample before testing.
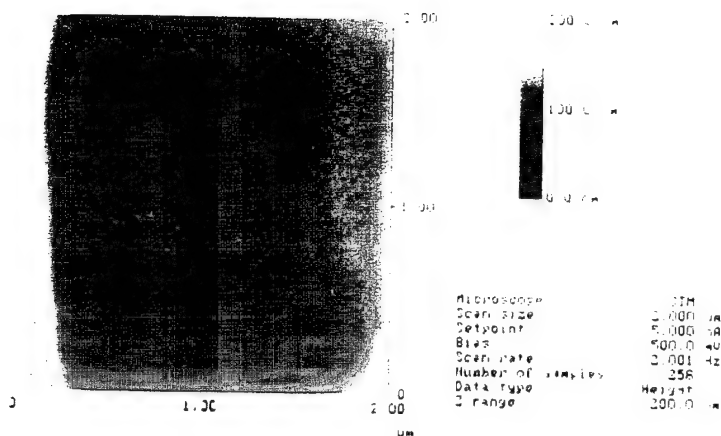
Figure 5b. DLC sample after 5 scans at 29µN imaging force. Note significant damage to surface.
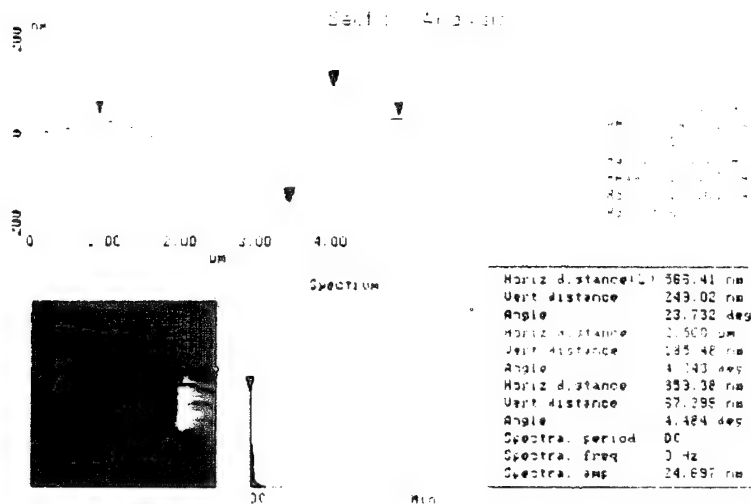
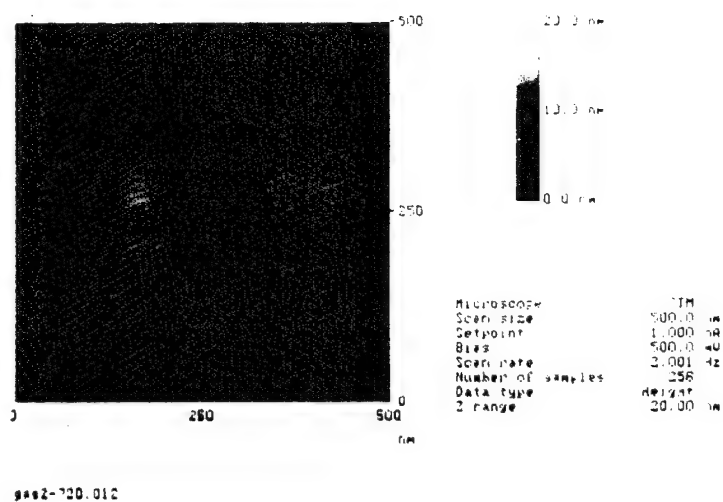Figure 5c. Sectional analysis of 5µm region centered on 2µm region scanned in figure 5b.

12

Microscope   STM
Scan size   500.0 nm
Setpoint   1.000 nA
Bias   500.0 mV
Scan rate   2.001 Hz
Number of samples   256
Data type   Height
Z range   20.00 nm

gaas2-720.012

Figure 6a. Indent (to provide visual reference) in GaAs surface

Microscope   STM
Scan size   500.0 nm
Setpoint   1.000 nA
Bias   500.0 mV
Scan rate   2.001 Hz
Number of samples   256
Data type   Height
Z range   20.00 nm

gaas2-720.013
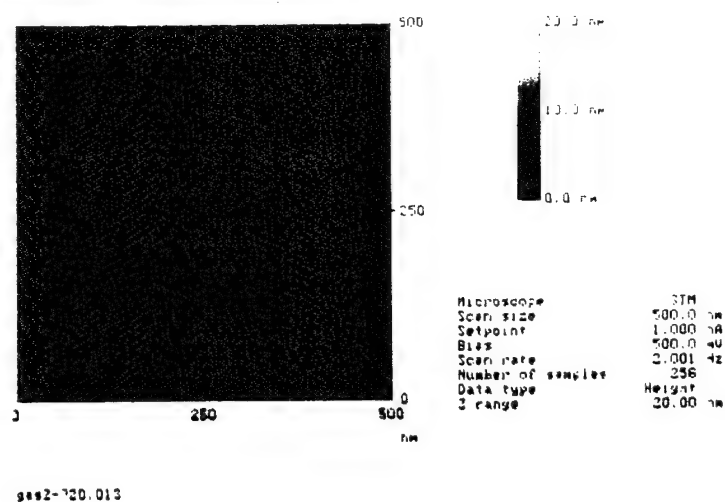
Figure 6b. Repeated scan of above, showing image stability of better than 25nm with new base.

13

very little shifting of the image from scan to scan, less than 25nm. The diagonal noise pattern is more prominent in these two images due to the displayed Z range being smaller, just 20nm, compared to other images such as figure 5a, with has a Z-range of 100nm.

Bare Lexan Polycarbonate was tested in the same manner as the DLC film, but at lower force levels. The first test was run at 0.86µN (0.088mg). **Figure 7a** shows a three dimensional representation of the 5µm region around the original 2µm region after it was scanned five times at 0.86µN. This image was taken on the sixth scan, immediately after the last scan of the 2µm region. **Figure 7b** shows a cross sectional analysis of the damage on the 2µm region. It seems that most of the damage occurs at the start of each scan line, with material being dug out there and pushed over to the end of the scan line. The depth of the trench visible in figures 7a and 7b is 5.5nm (55Å), and the height of the piled up material at the end of the scan lines is 17nm (170Å). There does not seem to be any significant removal of material from the center of the 2µm region.

Figure 8a shows a three dimensional representation of a Lexan surface where the force during the five 2µm scans was 2.7µN (0.28mg). The results are similar to the case at 0.86µN, but the amount of material displacement is larger, as expected. Also, there is a small but noticeable decrease in the height of the central 2µm area, rather than just at the beginning of the scan lines as in the lower force case. **Figure 8b** shows the cross section analysis of the results. The depth of the trench at the beginning of the scan lines is 25nm (250Å) and the height of the pile up at the end is 30.5nm (305Å).

Although there is some damage to the bare Lexan surface, the level of material displacement is low enough to not significantly affect the results of a scratch test in DLC films. After five scans at slightly higher than the minimum imaging force we can operate at now, the material height displacement was about 10% of the DLC film thickness of interest, so that in the case of a scratch test resulting in DLC film removal, the area of delamination will be clearly visible.

These tests clearly show that the DLC coated Lexan is far more resistant to mechanical surface damage than bare Lexan.

A GaAs wafer sample was also tested. **Figure 9a** shows a 5µm region centered on a 2µm region that had been scanned 5 times at 1.2µN imaging force without any visible damage. **Figure 9b** shows a 3-D view of a new area where the 2µm region was scanned 5 times at 2.5µN (0.26mg) this time there was definite damage. **Figure 9c** shows a section analysis of the image in 9b showing the wear depth to be about 10nm (100Å) deep.

As a general purpose test device for other materials, it would be desirable to reduce the imaging force, but it is possible to test most materials now by taking care not to make unnecessary, repetitive scans of the surface. On delicate materials, damage can be minimized by either withdrawing the tip after getting the desired image, or moving to a small region of the sample set aside for that purpose (similar to the "landing" or "parking" zone on a disc drive).
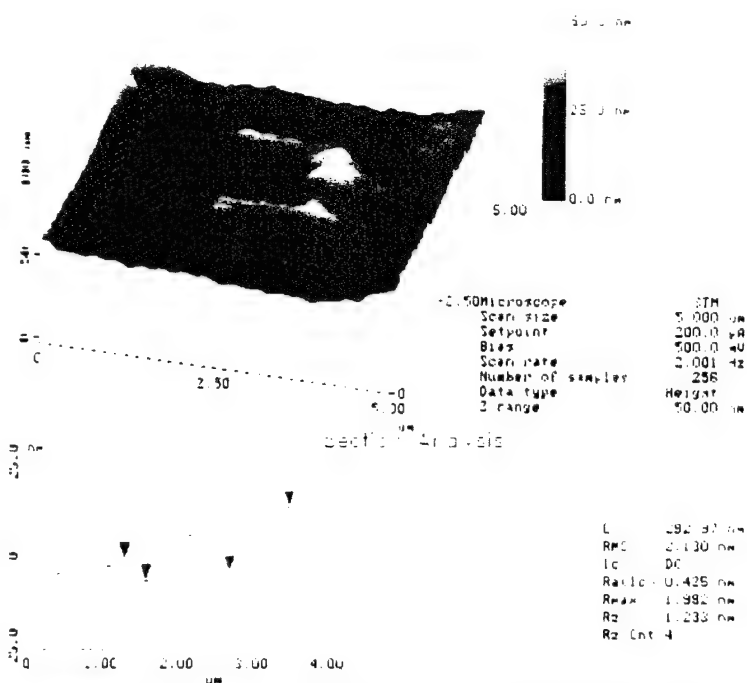
14

Figure 7a. 3-D view showing surface damage to bare Lexan caused by 5 scans at 0.36μN imaging force.
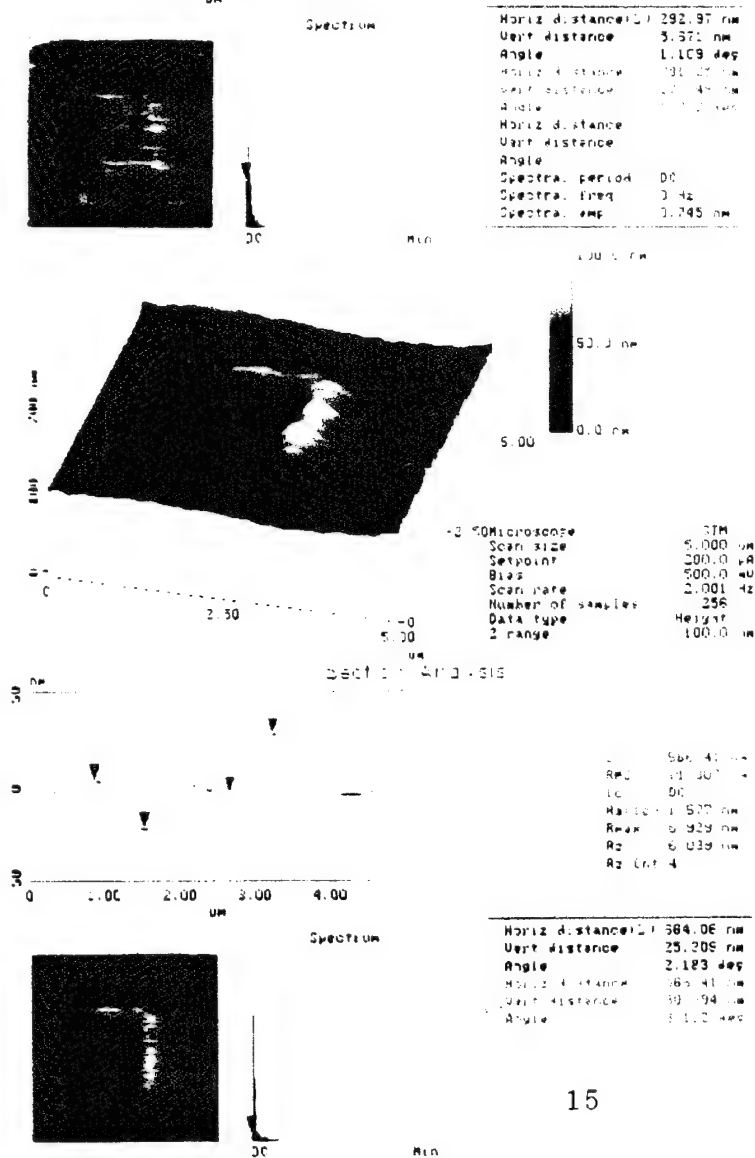
Figure 7b. Section analysis of worn area from figure 7a.

Figure 8a. 3-D image of worn region in Lexan surface caused by 5 scans at 2.7μN force.

Figure 8b. Section analysis of region shown in 8a, showing amount of material displacement.
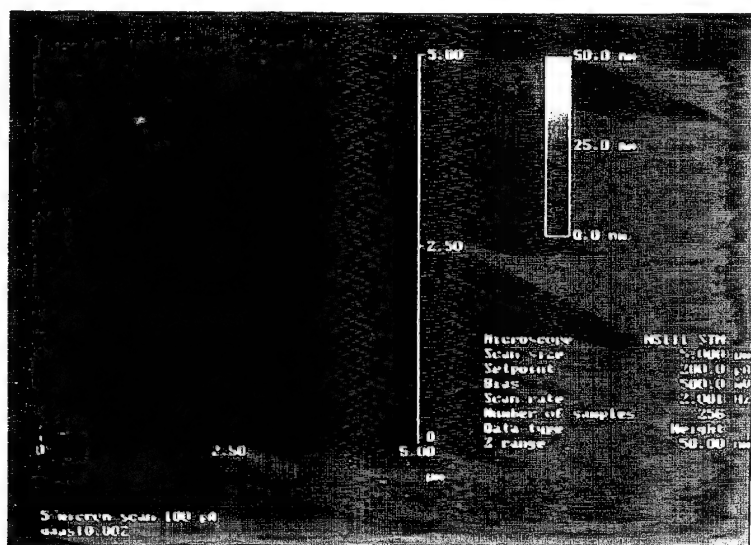
15

Figure 9a. 5μm image of GaAs surface. The 2μm region in the center was scanned 5 times at a force of 1.2μN, but no damage is visible.
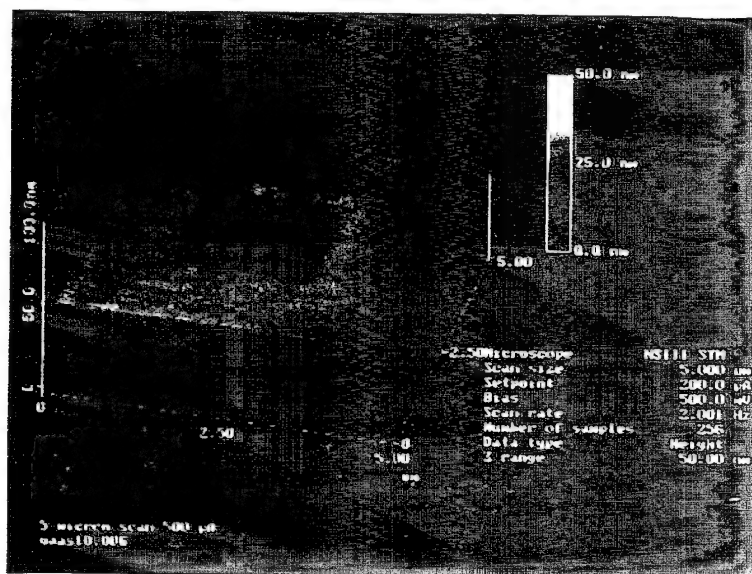

Figure 9b. 3-D view of GaAs surface similar to 9a above, except the force during the 5 scans of the central 2μm region was 2.5μN. Damage is obvious.
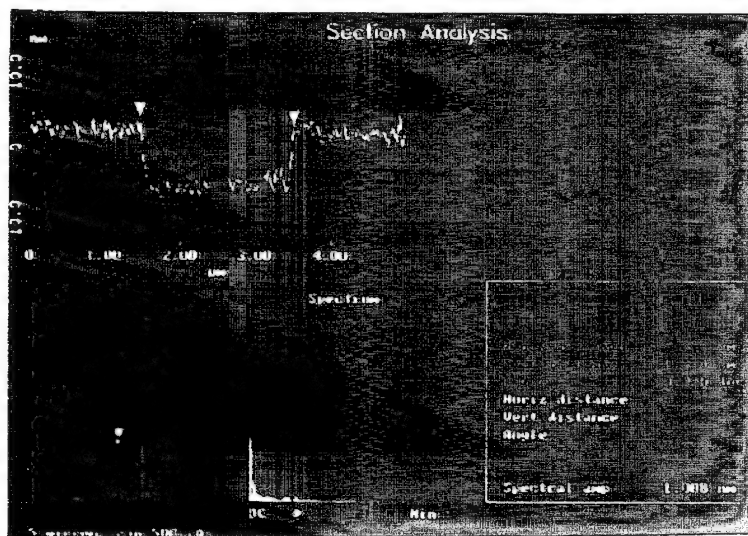
Figure 9c. Section analysis of 9b, showing depth of damage to be about 10nm.

16

Indentation Testing Of DLC Films produced some interesting results and showed some effects that could possibly be useful in evaluating the performance of various protective coatings.

Figure 10a shows the force versus time data captured by the data acquisition system of a series of eight indents starting at 0.7μm and ending with 1.4μm commanded Z-axis piezo travel. The resulting indents are shown in Figure 10b. The first two indents, at the bottom center of the image, with forces of 8.8 and 9.9mg (86 and 97μN) are barely visible. The next four indents, with forces of 10.3 to 14.5mg (101 to 142μN) are much larger than the first two, but are all similar in size. The force curves for these indents all show a small force discontinuity at about 10mg (98μN). These discontinuities are shown in greater detail in Figure 10e. The last two indents were much larger than the others. The peak force for these indents was 15.5 and 16.3mg (152 and 160μN) Figures 10c, 10d show the last two indents in greater detail. The superior quality of these two images is due to scanning at 0.5Hz, rather than 2Hz, but the time required to generate an image at 0.5Hz is 8.5 minutes versus 2 minutes at 2Hz.
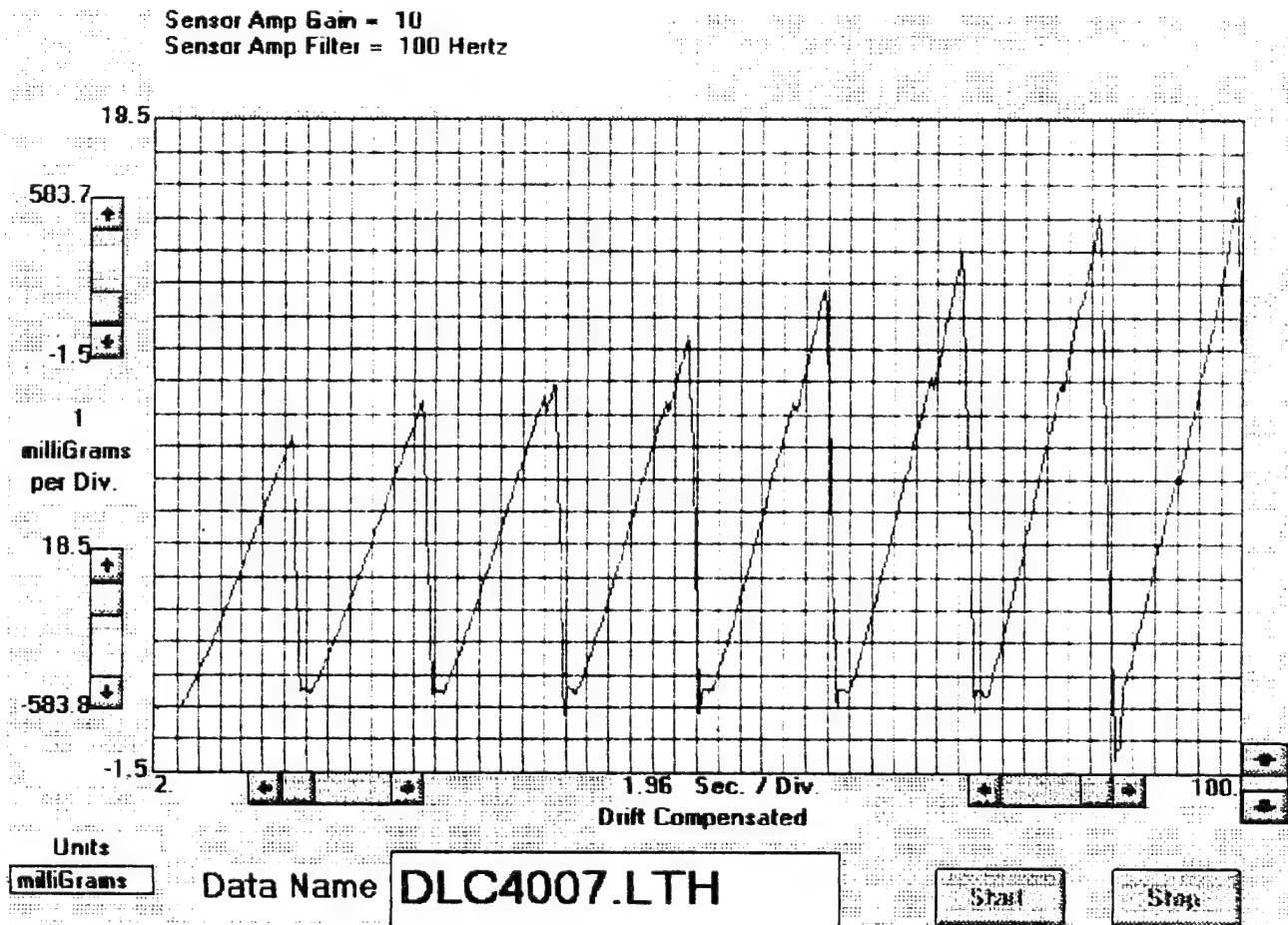

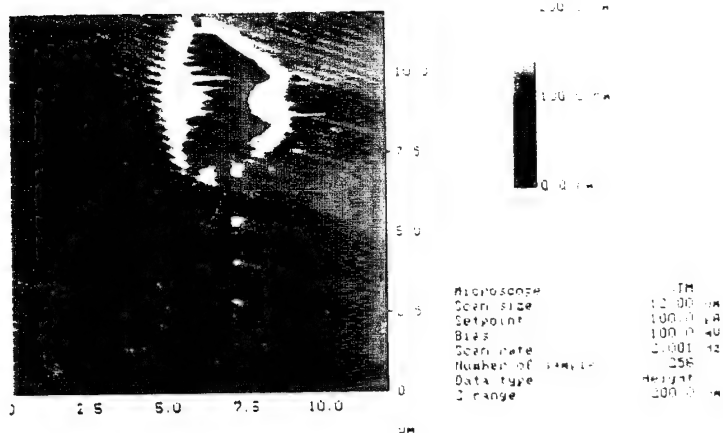Figure 10a. Force curves from series of 8 indents, at 0.7 to 1.4μm.

17

dtc4.003

dtc4.012

Figure 10b. Series of 3 indents from 0.7 to 1.4µm Z-axis travel.

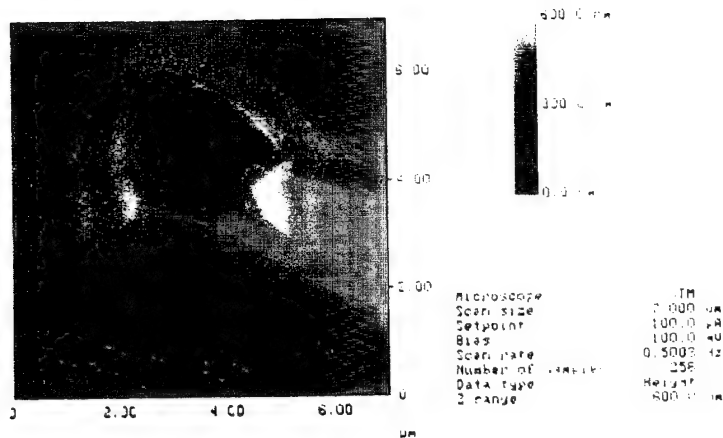**Figure 10c.** Close-up of indents from 1.3 and 1.4µm Z travel (15.5,16.3mg/152,160µN force).
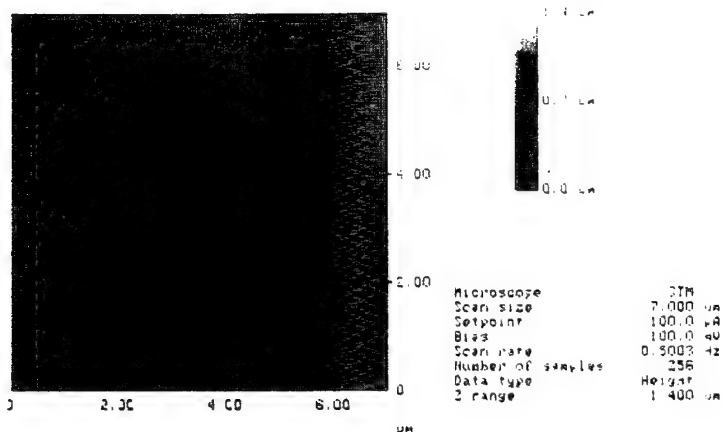
Figure 10d. Same as 10c, except greater displayed Z-range.
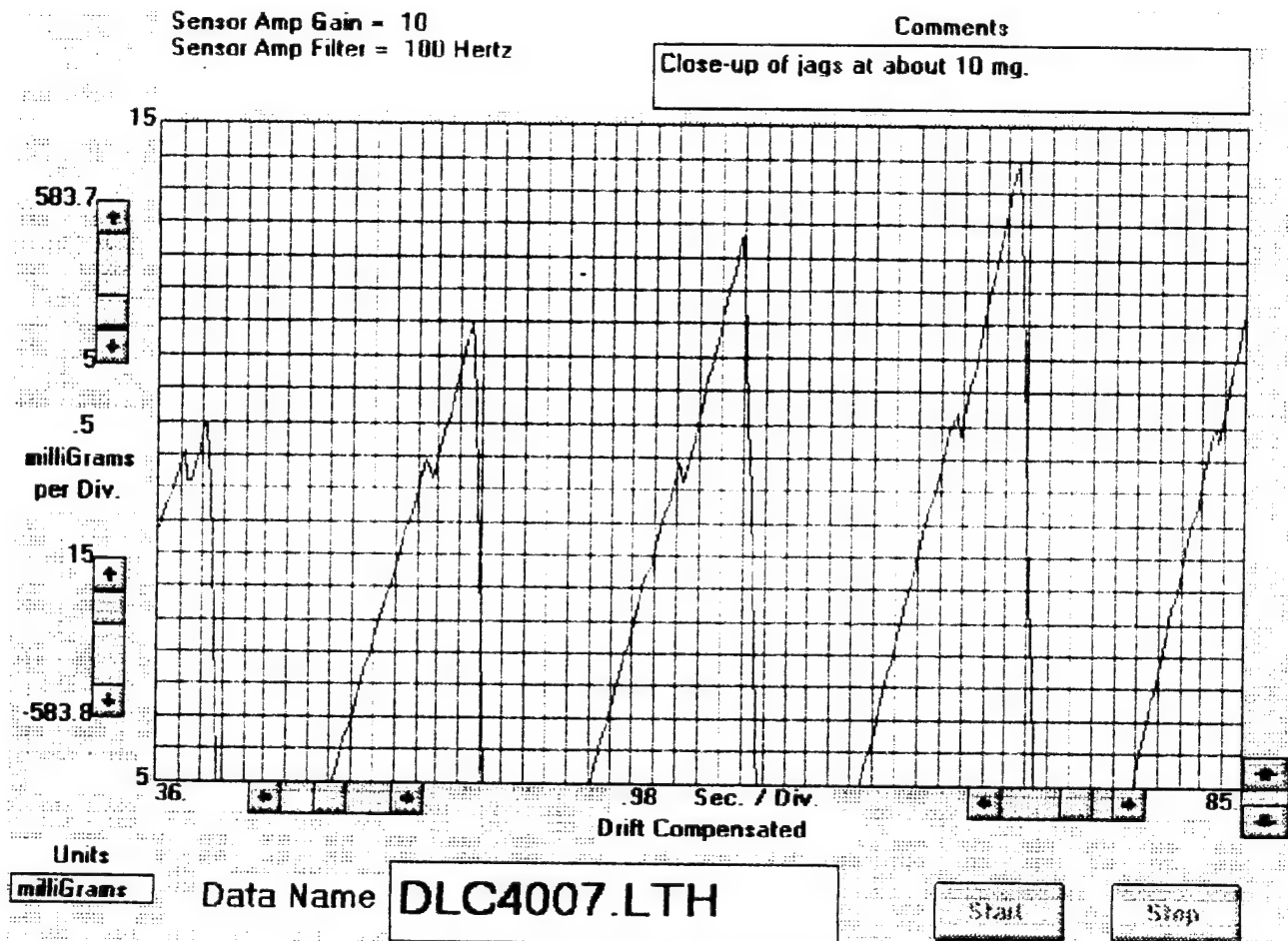
18

Figure 10e. Close-up of force discontinuities shown in 10a.

As discussed previously in the section on equipment, it was originally planned to obtain **load/displacement curves** by subtracting the sensor travel (given by the sensor output, with proper calibration factor) from the piezo travel to get the displacement of the tip into the sample. This was determined to be impractical, however, as the piezo travel did not follow the travel as prescribed in the lithography scripts accurately enough. Therefore, it was decided to implement **electrostatic actuation** of the sensor to provide the load force, rather than using the Z-axis piezo for that function.

To operate in this mode it was necessary to accurately know the sensor output versus position function, so the response of the sensor (SN 3MTS#5) was measured versus both load and displacement. Output versus load was tested using an Ohaus gram weight set. The system was then calibrated to read 200mV with a 200mg weight. Output versus position was then measured using a test fixture built for that purpose.

The test fixture consists of a rectangular frame of 0.5 inch thick by 4 inch wide aluminum plates holding a large barrel micrometer with 0.0001 in
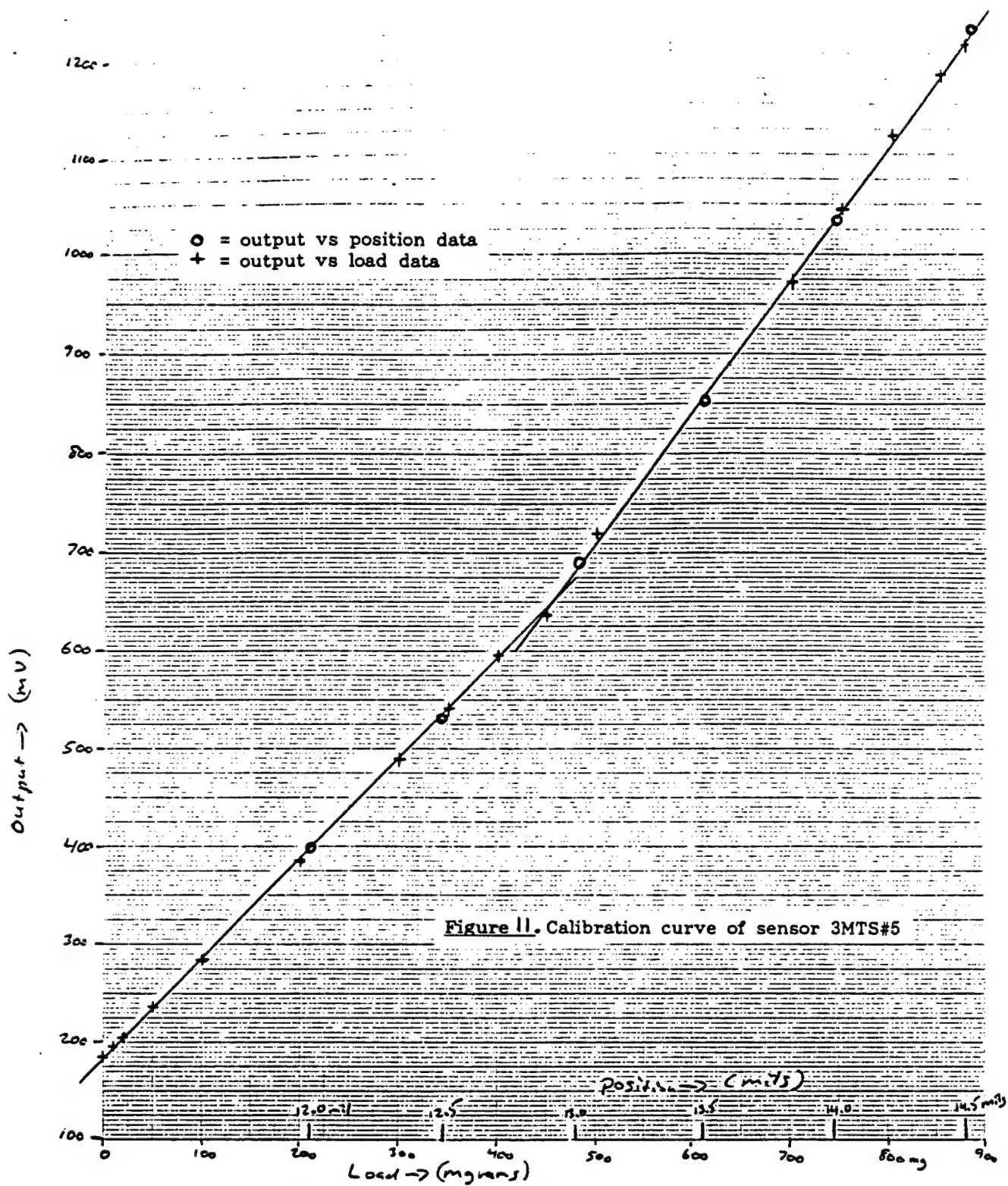
19

graduations so that the sensor can be inserted into the frame and the micrometer turned to bring the stem down onto the sensor. A 0.113 in diameter steel ball mounted on a 0.005 brass sheet was mounted onto the sample holder of the sensor to provide a precise contact surface. The ball was forced into the brass sheet to form a small dimple to help retain the ball, and to ensure that the dimple would be in firm contact with the sample holder to eliminate the possibility that the results would be affected by flexing of the brass sheet.

Figure 11. shows the plot of output versus mg load and output versus position. The output signal is absolute, that is, it was not adjusted to zero, in order to match the two curves together. The no load reading of the sensor was 186.9mV, and the reading with the steel ball was 400.5mV.

The horizontal scale for the position/displacement data was normalized to fit the mg load scale at 12 and 14 mils (1 mil= 0.001inch). The rest of the data points were then placed by calculating the load force expected from the displacement using the average spring constant between 12 and 14 mils of 267.5mg/mil. The curve shows a good fit between output versus load and output versus position, as was expected. A small anomaly in the response was also found: the change in slope of the response at about 450mg load. All measurements were made below 400mg absolute load, so this "kink" in the curve did not effect the measurement results. The spring constant was then determined from the data at 12.0 and 12.5 mil to be 256mg/mil or 10.1mg/μm (103μN/μm) in the region from 0 to 400mg load. Since the load calibration is 1mV/mg, the spring constant of 10.1mg/μm gives an output of 10.1mV per μm of displacement.

The kink in the calibration curve is believed to have been caused by the original method of producing the torsionally stabilized center electrode assemblies, which involved hand trimming with an X-Acto knife. During this trimming step, the spring arms were often bent slightly. The manufacturing process has since been improved to eliminate such accidental bending of the spring arms.

The sensor force vs electrostatic potential was measured at constant position by adding test weights and determining the voltage required to balance the force of those weights. This was done with a 150mg tare weight in place for all measurements, which is the same weight as the typical sample. After zeroing the reading, the test weights were applied in a series from 1 to 200mg, and the voltage required to return the scale reading to zero was recorded. With this method, the center plate is always at the same position, so the electric field is proportional to the applied voltage. The data is shown in **Figure 12.** It has been plotted as the square root of the resultant force versus the applied voltage, as this should theoretically give a straight line. The results are indeed a close fit to a straight line. The most significant deviation from the straight line is for the data point at 45 Volts. This is not a measurement error, it has been repeated several times. A probable explanation is that the deviation is caused by the combined effect of the 15 Volt drive plate signal superimposed on the electrostatic potential. This effect is only significant at very low loads, below about 50μN (5mg). At forces of above 50μN, the force can be accurately calculated as a constant times the square of the voltage, with the "constant" being valid for a fixed position of the sensor.
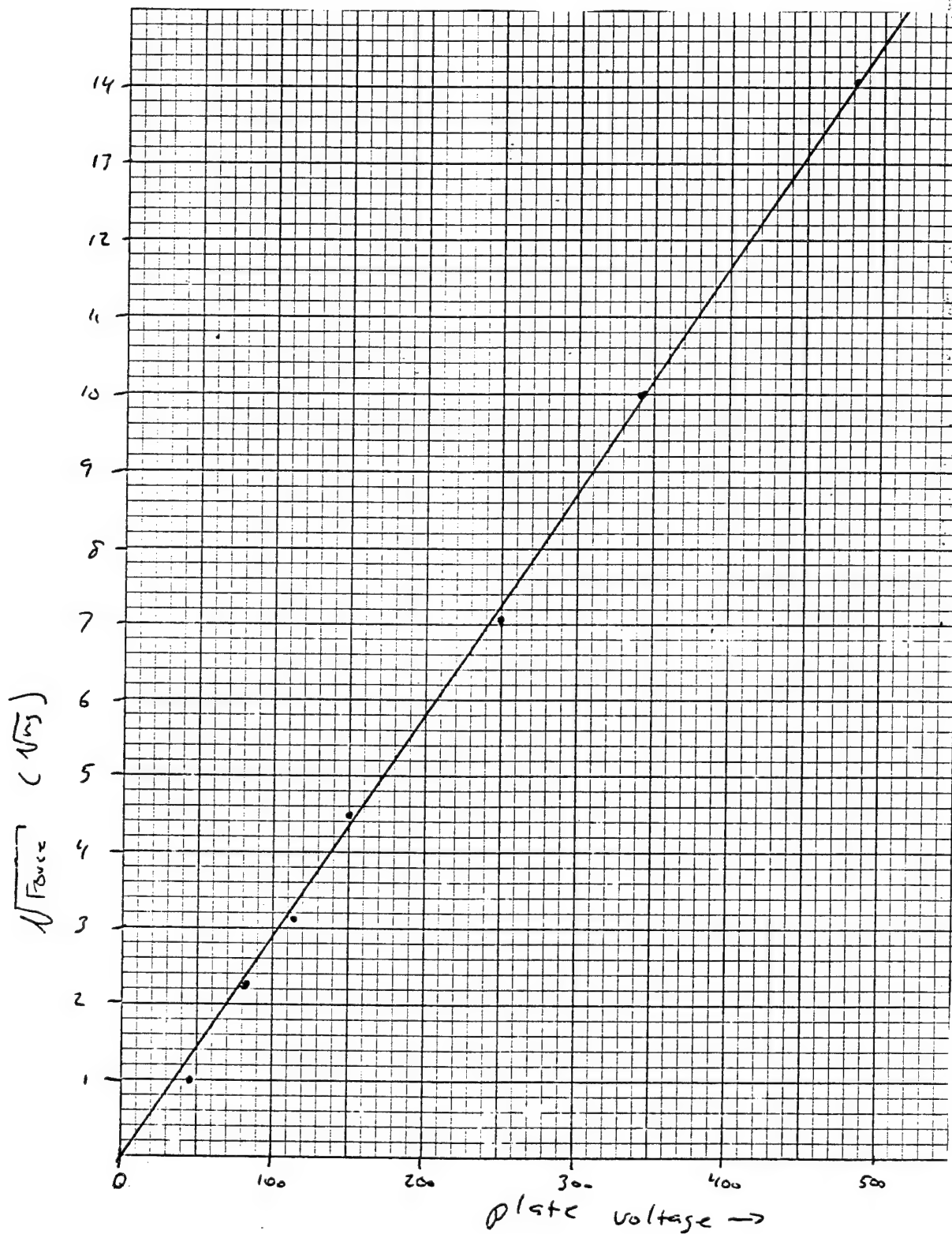
20

Figure 11. Calibration curve of sensor 3MTS#5

O = output vs position data
+ = output vs load data

Output ⟶ (mv)

Position ⟶ (mils)

Load ⟶ (mgrams)

21

Figure 12. Square root output force vs voltage

22

The force generated by electrostatic actuation can be calculated as:

$$F = KV^2 \quad \text{(V = voltage in Volts)}$$

Using the data point at 200mg (1.96mN), which required 483V to generate, the force constant K was calculated to be 8.40nN/V^2 (at 150mg static load).

The exact value of K will vary with the sample weight, as this changes the internal plate spacing in the sensor. In Phase II, this relationship will be determined so that the actual force on the sample can be determined for any combination of position (whether due to sample weight or deflection during indenting) and electrostatic voltage.

Ideally there would be no change in the sensor output with applied electrostatic voltage if the sample were held at a constant position. Testing did show a small change in output versus voltage, however. This undesired sensitivity was measured by placing the steel ball test sample, used previously for measuring output versus position, on the sensor, and placing a flat steel plate on the STM base, instead of the STM scanner. The adjustment screws in the STM base were set to put the sensor in the same position as with a 150mg sample. This was possible even though the steel ball test sample weights over 200mg, as the magnets in the adjustment screws caused a fairly strong attraction (over 1gram force) between the steel ball and the steel plate above it. The steel plate was 0.9cm thick, so deflection under the electrostatic loads of 2mN maximum would be negligible. The radius of curvature of the steel ball was 1.4mm, which is over 10,000 times the radius of the diamond probe tips, so elastic deformation should also be negligible. With this set up, it was assumed that the sensor position was held constant and that any change in output signal with applied voltage was an error signal. These output versus applied voltage curves were recorded using a triangular wave voltage with peak values of 100, 200, 300, 400 and 500V. Results of the 100 and 500V tests are shown in **figures 13a and 13b**. The simple triangular waveform is the applied voltage. The other waveform is the output signal.

As the electrostatic voltage is increased from 10 to 40 volts there is a sharp rise in the sensor output of 0.38mV (380mV at 1000X gain). This indicates a 38nm position change, but it is in the wrong direction, as the electrostatic force pulls the center electrode and sample up, so that motion caused be a compliant support system would result in a negative, rather than positive output. Careful observation of the sensor signals indicate that this part of the error is due to a loading change on the drive plate signal due to varying output impedance of the 500 volt amplifier with output voltage. This effect could be greatly reduced by reducing the output impedance of the plate drive integrated circuits, and also by increasing the value of the isolation resistor.

The rapid rise in signal output from 10 to 40 applied volts is followed by a more gradual decline from 40 to 140 volts. This could be due to elastic deflections as it is in the expected direction for this. Further attention to the mounting of the sensor to minimize the possibility of elastic deflection could determine if this is the case.
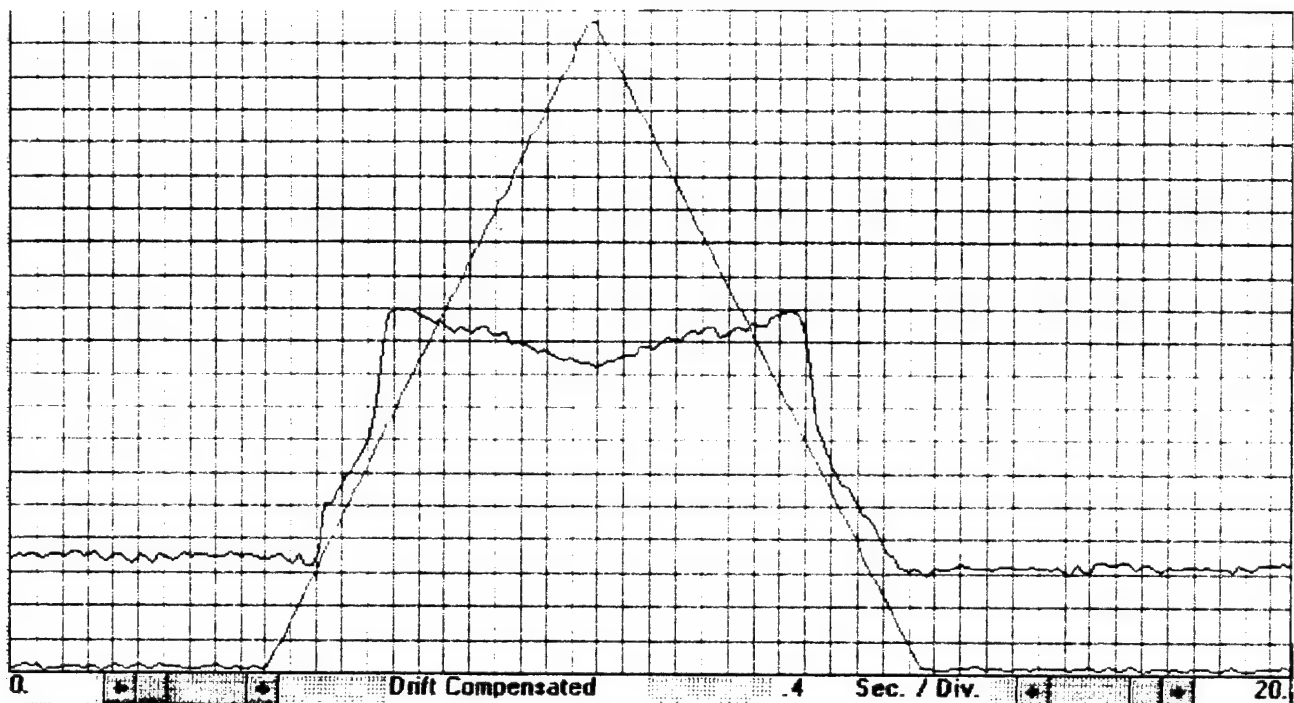
23

Figure 13a. Displacement error calibration at 100V. Scale factor for displacement is 5nm per division.
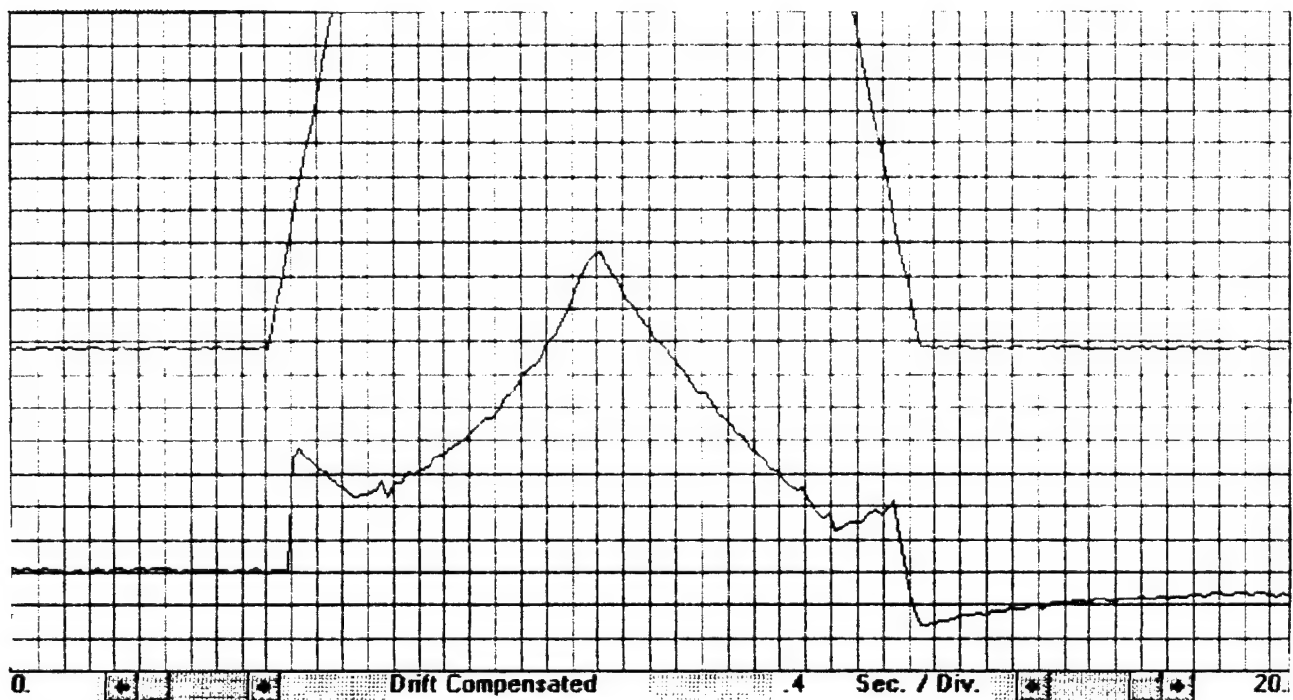

Figure 13b. Displacement error calibration at 500V. Scale factor for displacement is 10nm per division.

24

Above 140 volts the signal rises again, to a peak of 0.96mV (960mV at 1000X) which is equivalent to 96nm. Measurement of internal sensor signals showed a change in the DC bias level of the center electrode of about 5.5mV over this range. This small DC level shift would not effect the output signal by itself, but it does indicate that there is a small amount of current flowing from the drive plate to center electrode at high applied voltages. If this is due to corona discharge, ionized air inside the sensor could vary the relative capacitance between the sensor plates and cause an erroneous output signal variation. If this is the cause, it could be eliminated be filling the sensor with a dielectric fluid to prevent corona breakdown. This would also increase the available force in proportion to the dielectric constant of the fluid.

The last, and perhaps most important potential error is the hysteresis, or how close the reading before and after the loading cycle match, in the absence of plastic deformation of the sample. This is because that error determines the accuracy with which it is possible to determine the plastic indent depth, which is commonly used as the main measurement value to characterize the indent. **Figure 13a** (100V/84µN peak) shows approximately 1nm of hysteresis. **Figure 13b**, at the much higher load of 2.1mN peak, showed a total error due to hysteresis and viscoelastic effects of approximately 7nm when measured 5 seconds after the end of the loading cycle. A similar effect has been observed in testing sensors loaded normally with weights. We believe the source of this effect to be deflection of the epoxy/glass fiber material used in the outer layers of the sensors. Materials changes described in the Phase II work plan to reduce temperature sensitivity will also provide nearly perfect elastic response, compared to the present material.

Time did not permit implementing any of the proposed methods for reducing the error, but the error curves have been used to correct the recorded indent data for several tests on GaAs. This allowed direct comparison with results from the IBM indenter. Curves of displacement and applied electrostatic voltage versus time for indents in GaAs are shown in **figure 14a** (400V/1.34mN peak load) and **figure 14b** (500V/2.10mN peak load). The load force was calculated from the previously determined force constant of $8.40nN/V^2$, at 50 volt intervals of the electrostatic potential. The error component of displacement, as recorded in figures 13a and 13b, were subtracted from the displacement data, and the resultant data was plotted as load versus displacement depth. **Figures 15a and 15b** show the load/displacement curves obtained using the Hysitron instrument, with peak loads of 1.34mN and 2.10mN, respectively. **Figures 16a and 16b** show results from the IBM indenter on the same GaAs material at similar loads of 1.3mN and 2.05mN. Edge Technologies tip #3 was used for all of these tests.
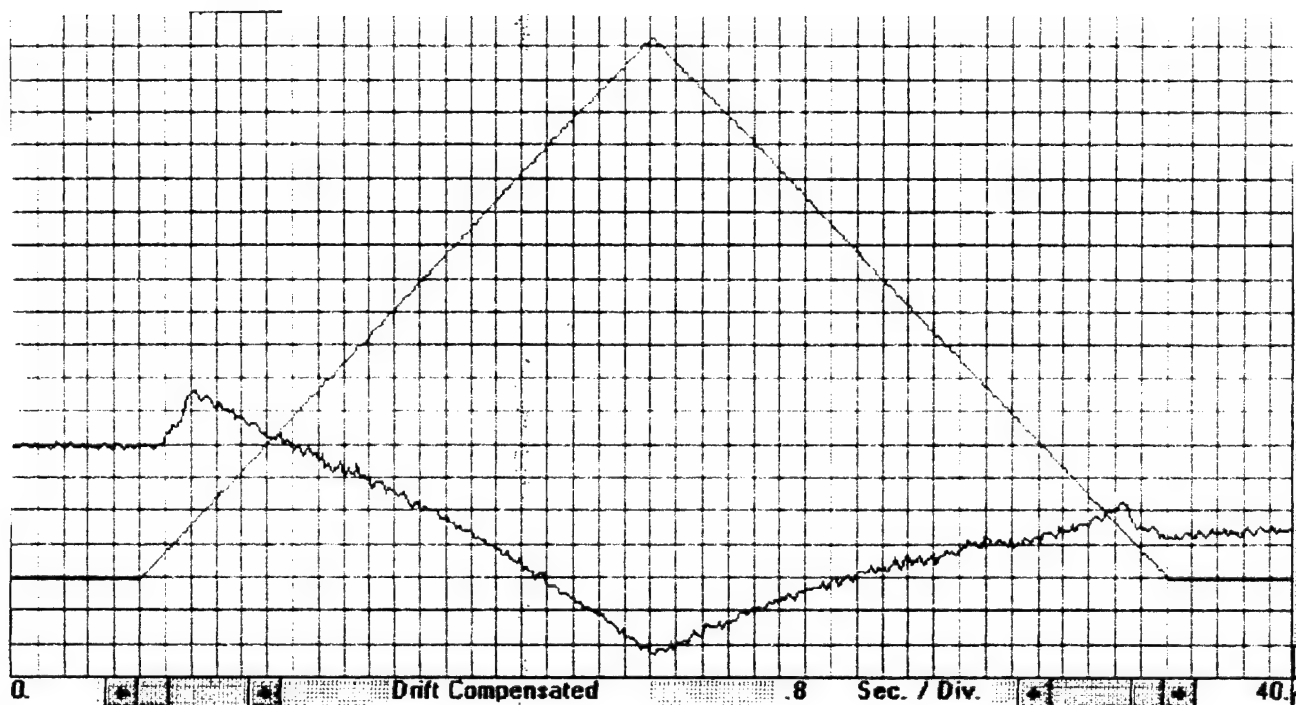
Figure 14a. Indent data for GaAs at 400V peak (1.34mN). Displacement scale is 25nm per division.
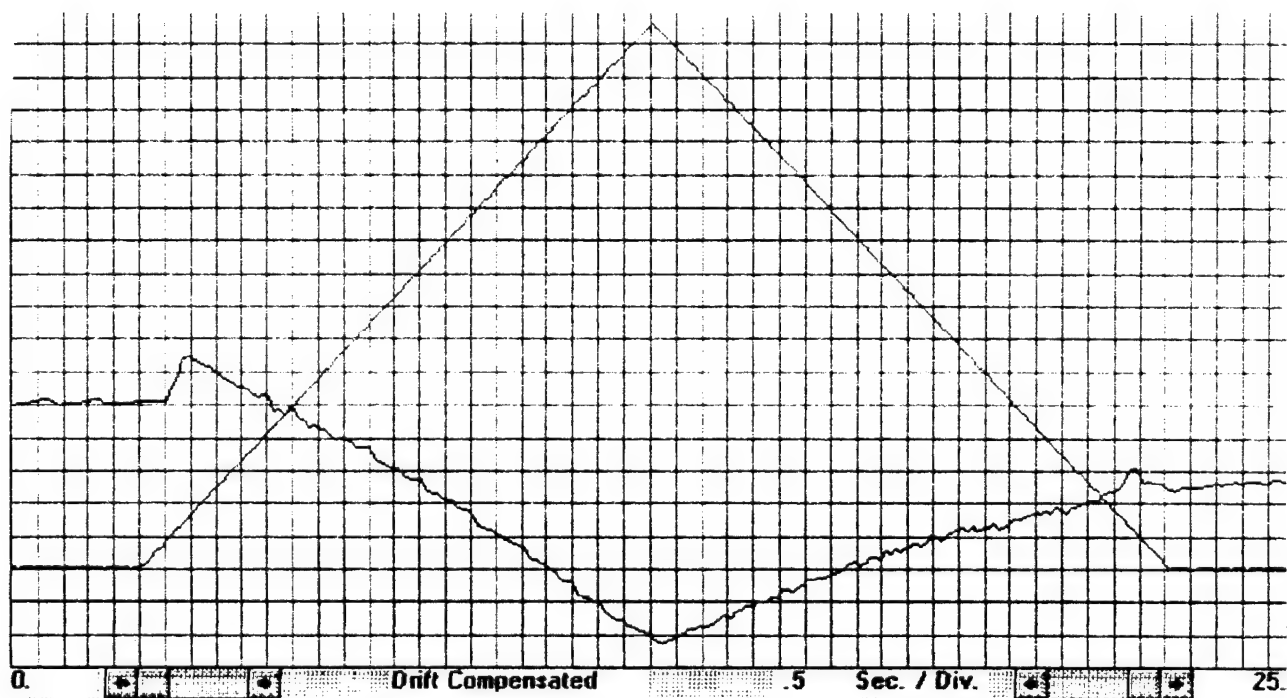

Figure 14b. Indent data for GaAs at 500V peak (2.10mN). Displacement scale is 30nm per division.
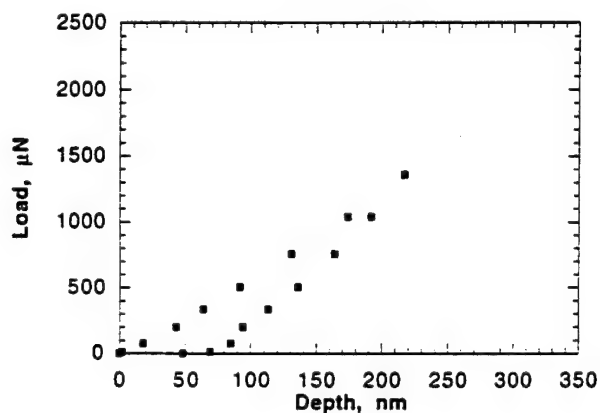
26

Hysitron, Inc. / 7-Sigma
Nanoindenter

Figure 15a. Hysitron load/displacement curve
1.34mN peak load

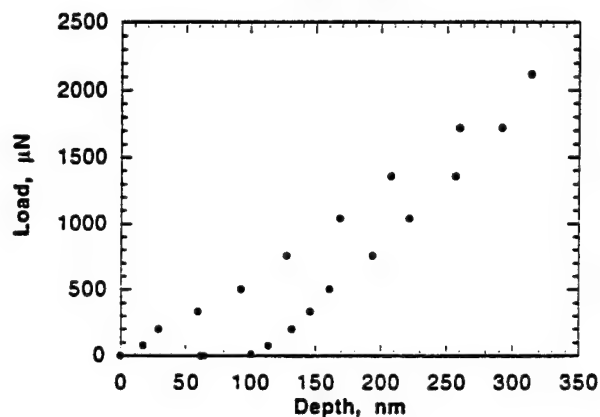## Hysitron, Inc., / 7-Sigma
Nanoindenter

Figure 15b. Hysitron load/displacement curve
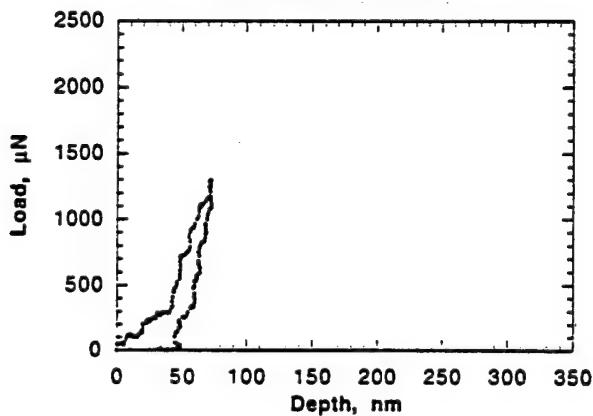2.10mN peak load

IBM Nanoindenter

Figure 16a. IBM load/displacement curve
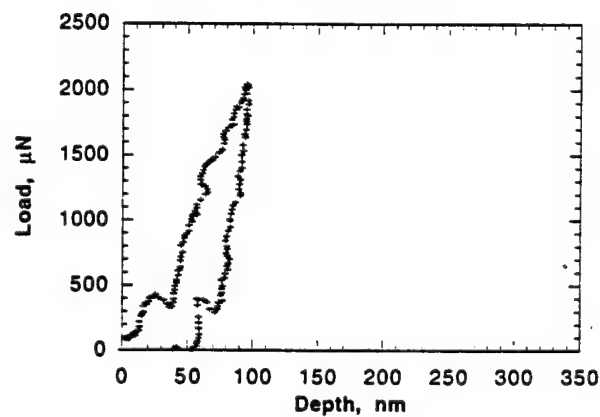1.3mN peak load

IBM Nanoindenter

Figure 16b. IBM load/displacement curve
2.05mN peak load

27

The IBM load/displacement curves are rather noisy at these low loads, and show some behavior that is definitely not the actual behavior of the material. In particular, figure 16b shows a decrease in the penetration depth on the loading curve of about 10nm as the loading force is increased from 1250 to 1325μN. The decrease in load force from 400 to 300μN as the depth increases from 25 to 40nm is possibly real, but the same shaped "wiggle" in the curve on the unloading cycle is almost certainly not real.

When the IBM indenter load force is unloaded, the tip may come out of contact with the sample, and the curve shows data points at zero load moving back towards zero depth. This, along with the noise effects, result in the plastic indentation depth being most accurately determined by drawing a best fit line through the unloading curve and taking its intersection with the depth axis as the plastic indent depth. This gives indent depths of 60nm for the 2.05mN load and 50nm for the 1.3mN load.

The Hysitron indenter was set up to leave the tip in contact with the sample, at a very small force, after the load was released. This allows the plastic indent depth to be more readily determined, as the last data point on the curve is the plastic indent depth. **Figures 15a and 15b** show the load displacement curves obtained using the Hysitron system. For 2.10mN peak load the plastic depth was 62nm and for 1.34mN the depth was 48nm. This is in very good agreement with the IBM results.

The elastic slope of the Hysitron results indicate a more compliant system than in the IBM instrument. This does not effect the measurement of plastic indent depth, but it does interfere with determining such things as elastic modulus. It appears that the tip mounted on the piezo is not being held at a constant height during indenting. The area of the piezo scanner tube holding the tip has 30,000,000 times more area than the contact area during a 1μm diameter indent, but the tip is not attached directly to the scanner tube. It is held by a metal tube similar to a hypodermic needle that is epoxied to a small ceramic crossbar mounted on the piezo tube. This mounting system was indented for use with an STM, where there would not be any intended contact between the tip and the sample. In Phase II the source of this compliance will be determined and reduced as much as possible.

Images of the above indents done on the Hysitron system are shown in **figures 17a and 17b.** The ridge clearly visible through the center of figure 17a, and barely visible in figure 17b corresponds with a small scratch or fracture on the diamond tip that was observed during SEM inspection.
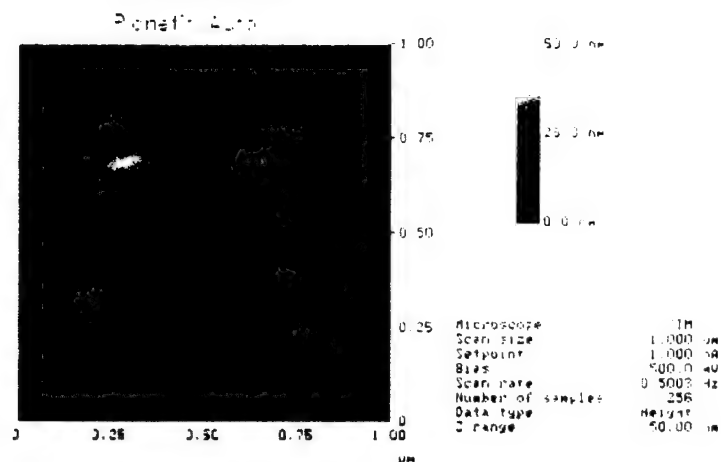
28

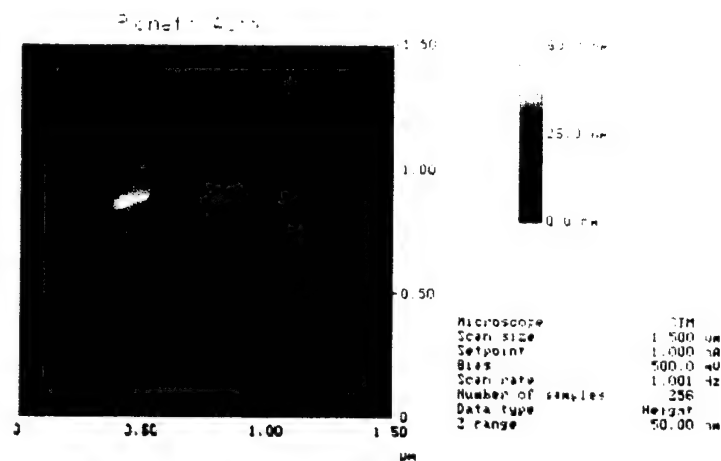**Figure 17a.** Indent in GaAs surface at 400V (1.24mN). Length of lower right edge is 0.65μm.

Figure 17b. Indent in GaAs at 500V (2.10mN). Length of lower right edge is 0.75μm.

Scratch testing has also been performed using 1000Å DLC on polycarbonate and 1000Å Chrome on fused silica. All of these tests were performed with Edge Tech tip #3, and force was applied using lithography scripts in the same manner as the previous scratch tests of several months ago, except that the number of steps was increased from 5 to 20 or 25, to more closely approximate the desired continuous increase in load as the tip is translated sideways.

It will be possible to use electrostatic actuation to apply the load during the scratch testing also, which will allow producing the desired continuously increasing load force, as well as providing a much larger maximum force. It was not possible to do that in the time available, but all that is required to implement it is a small amount of additional programming to synchronize the lithography script to the data acquisition and control system. This will also provide penetration depth data for the scratch test, as is now available for indents run in electrostatic actuation mode.

Figure 18a shows the load force versus time for an 8µm long scratch in DLC. The peak load was 121µN (12.3mg). **Figure 18b** shows the image of the results. **Figures 19a and 19b** show the same thing except the peak force was 172µN (17.5mg). Notice the large indent at the end of this scratch. This behavior is similar to the indent data presented in previous reports, where the plastic indent size increased dramatically at a certain load. That load is about 70% higher in the present case, which is probably explained by the shallower facet angles on the present tip.

Figures 20a and 20b show scratch results for a chromium film on fused silica. The peak load was 142µN (14.5mg), and the scratch length was 5µm. The yellow circle at the end of the scratch (near the top of the 20b image), is believed to indicate the beginning of delamination of the film from the substrate. **Figures 21a and 21b** show another test on the chrome sample at the higher load of 298µN (30.4mg). In this case the delaminated area is many times larger.
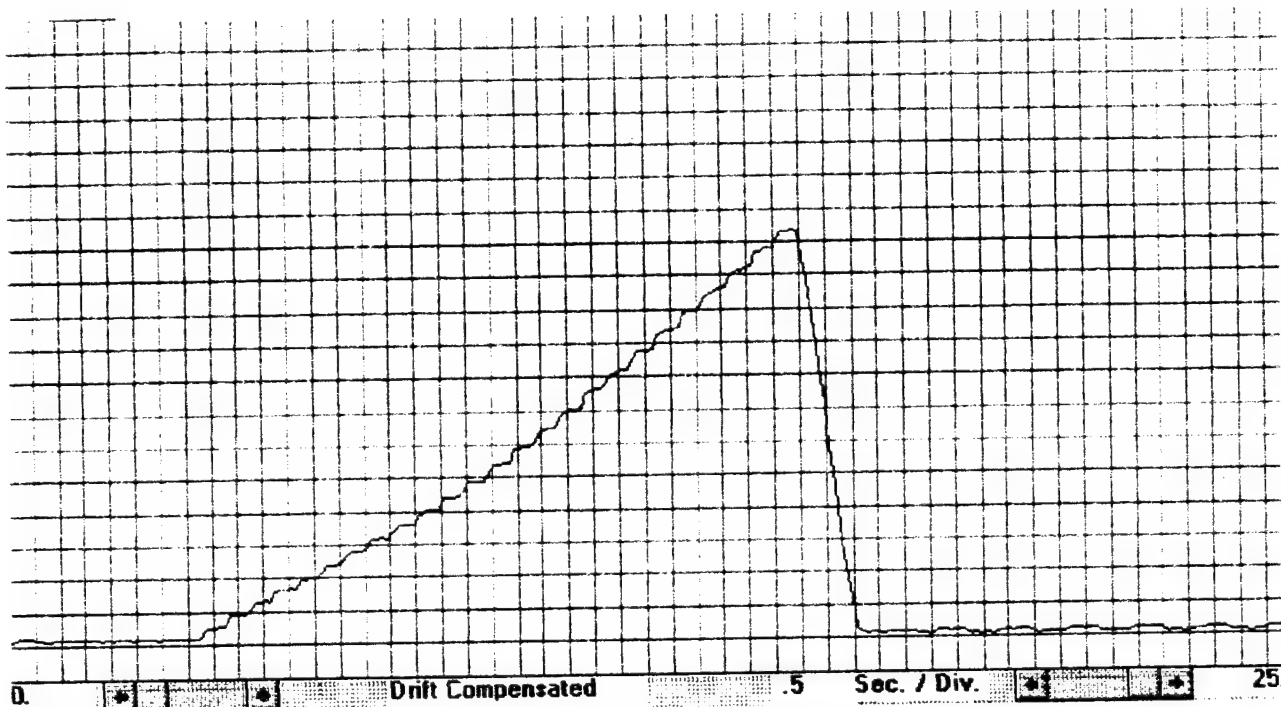
Figure 18a. Force data from 8μm long scratch in DLC. Peak load is 121μN. (vertical scale 1mg/div.)
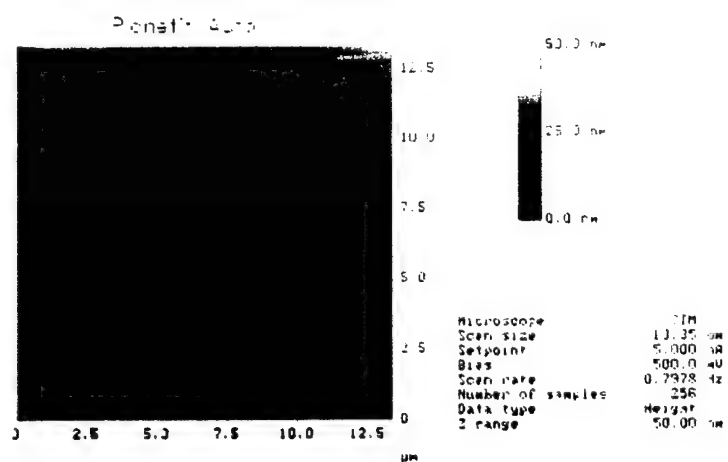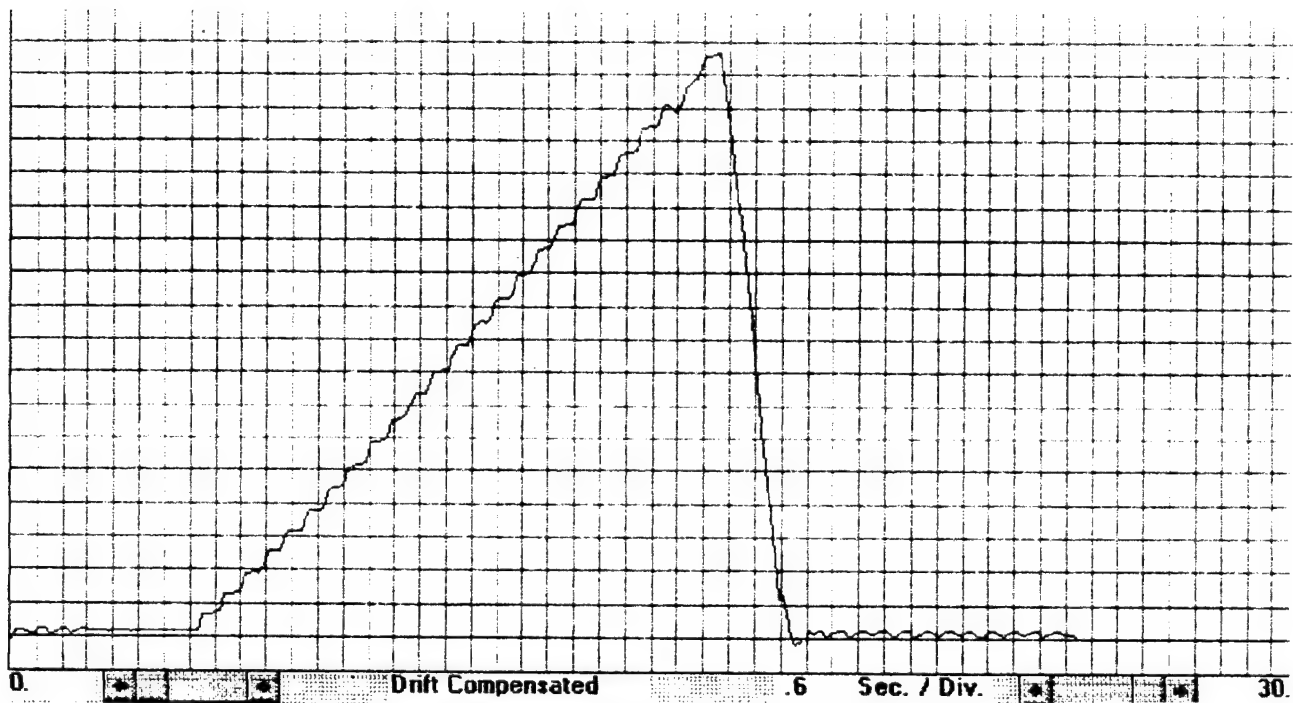

Figure 18b. Image of above scratch

31

0. | Drift Compensated | .6 | Sec. / Div. | 30.

Figure 19a. Force data from 8µm long scratch in DLC. Peak load is 172µN. (vertical scale 1mg/div.)

Figure 19b. Image of above scratch

Microscope	STM
Scan size	13.59 um
Setpoint	5.000 nA
Bias	500.0 mV
Scan rate	0.7978 Hz
Number of samples	256
Data type	Height
Z range	50.00 nm

dlc-8:5 C04

32

Figure 20a. Force data from 5μm long scratch in chrome. Peak load is 142μN. (vertical scale 1mg/div.)
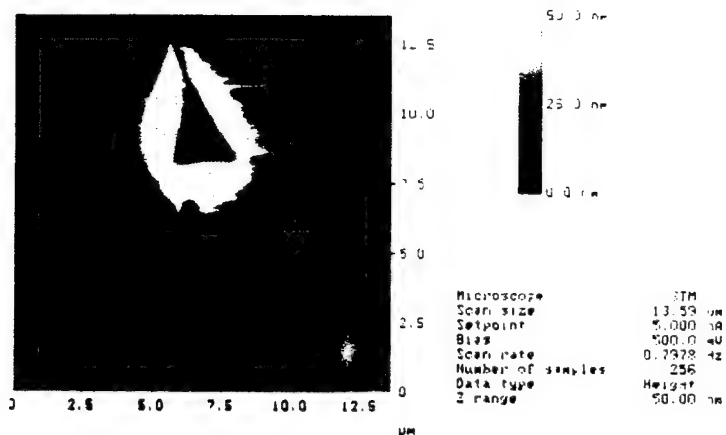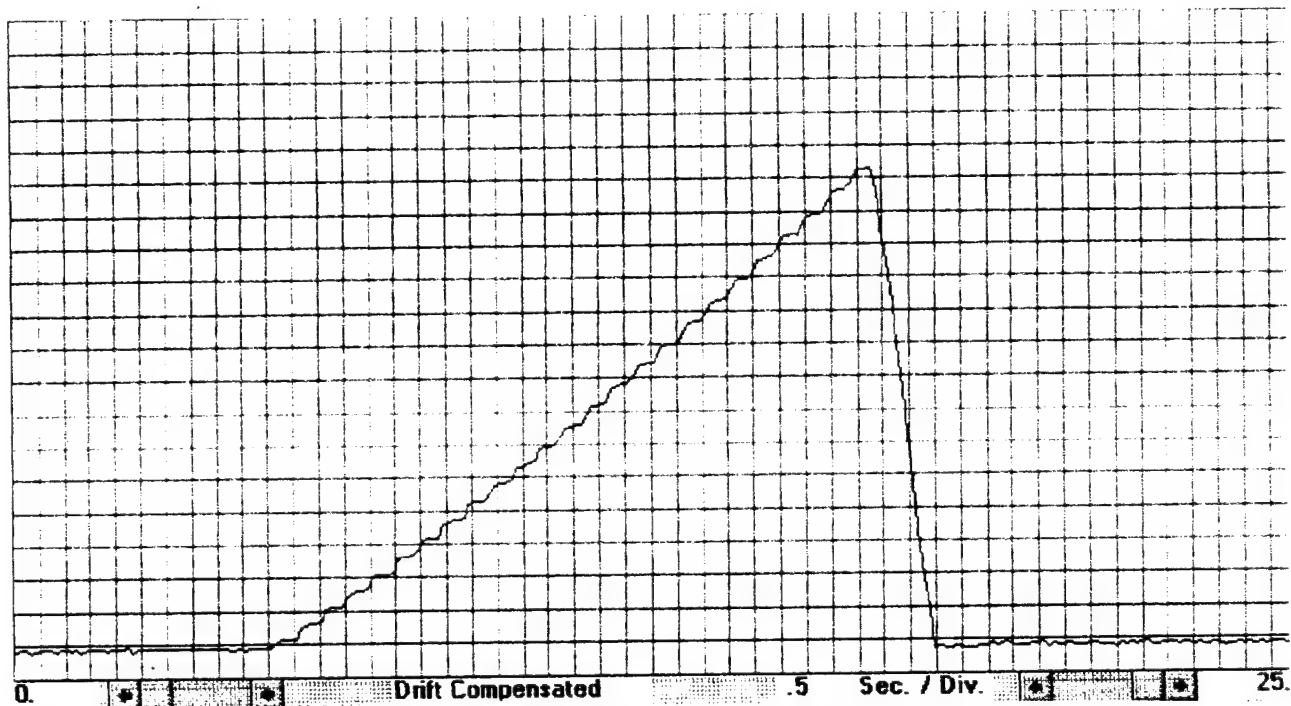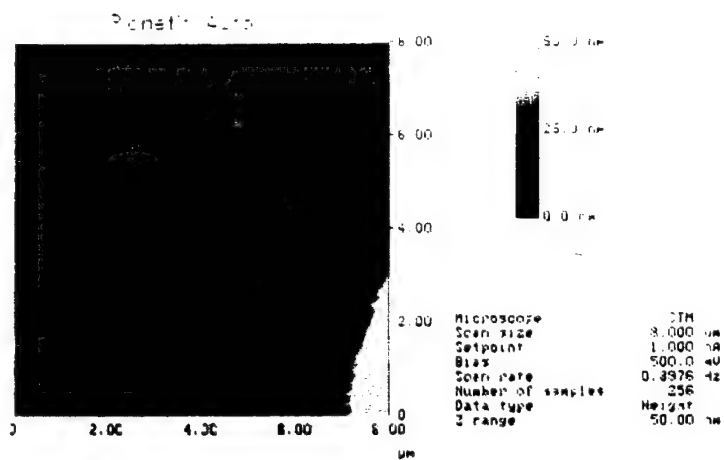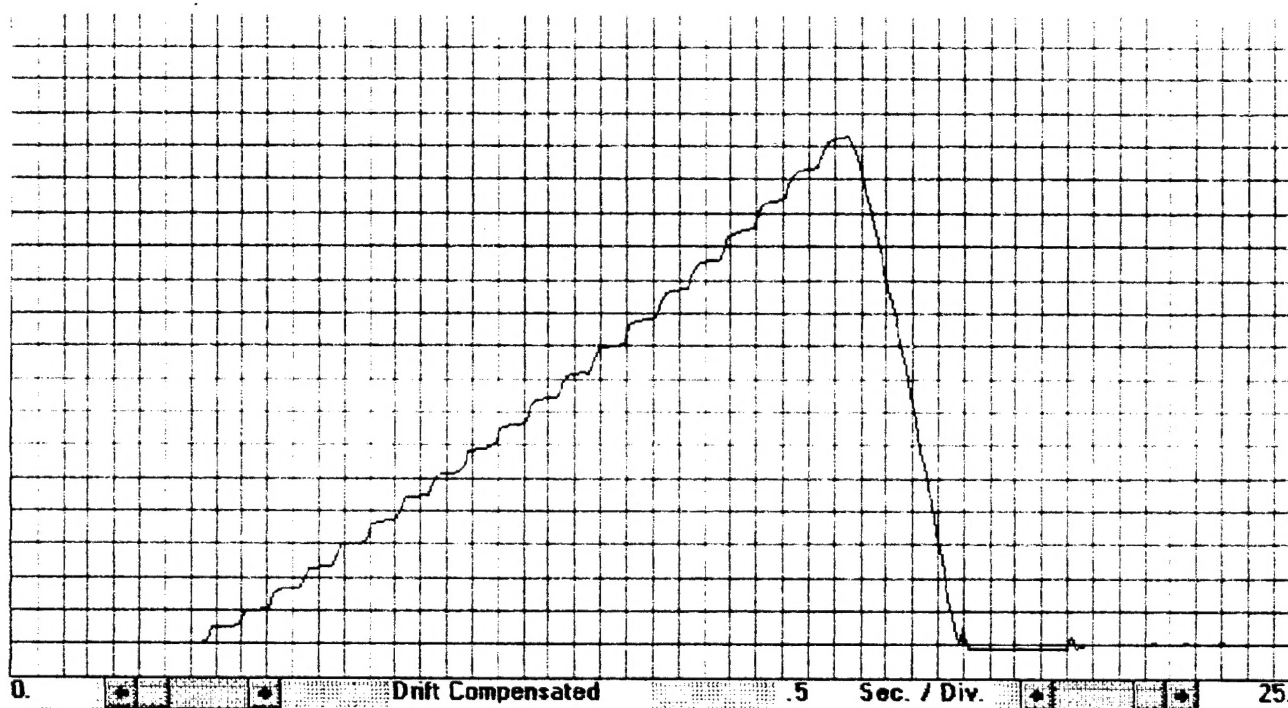

Figure 20b. Image of above scratch

chr-919 C02

33

Figure 21a. Force data from 5μm long scratch in chrome. Peak load is 298μN. (vertical scale 2mg/div.)
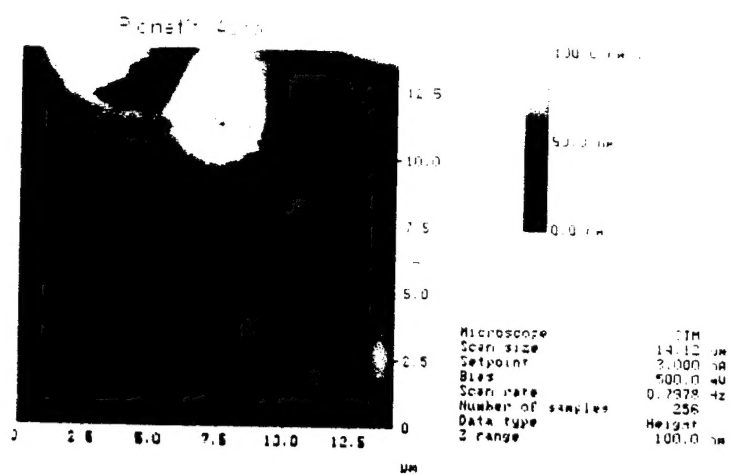

Figure 21b. Image of above scratch

34

DISTRIBUTION LIST

No. of Copies	To

1   Office of the Under Secretary of Defense for Research and Engineering, The Pentagon, Washington, DC 20301

    Director, U.S. Army Research Laboratory, 2800 Powder Mill Road, Adelphi, MD 20783-1197
1   ATTN: AMSRL-OP-SD-TP, Technical Publishing Branch
1   AMSRL-OP-SD-TA, Records Management
1   AMSRL-OP-SD-TL, Technical Library

    Commander, Defense Technical Information Center, Cameron Station, Building 5, 5010 Duke Street, Alexandria, VA 23304-6145
2   ATTN: DTIC-FDAC

1   MIA/CINDAS, Purdue University, 2595 Yeager Road, West Lafayette, IN 47905

    Commander, Army Research Office, P.O. Box 12211, Research Triangle Park, NC 27709-2211
1   ATTN: Information Processing Office

    Commander, U.S. Army Materiel Command, 5001 Eisenhower Avenue, Alexandria, VA 22333
1   ATTN: AMCSCI
1   AMCMI-IS-A

    Commander, U.S. Army Materiel Systems Analysis Activity, Aberdeen Proving Ground, MD 21005
1   ATTN: AMXSY-MP, H. Cohen

    Commander, U.S. Army Missile Command, Redstone Arsenal, AL 35809
1   ATTN: AMSMI-RD-CS-R/Doc

    Commander, U.S. Army - ARDEC, Information Research Center, Picatinny Arsenal, NJ 07806-5000
1   ATTN: AMSTA-AR-IMC, Bldg. 59

    Commander, U.S. Army Natick Research, Development and Engineering Center Natick, MA 01760-5010
1   ATTN: SATNC-MI, Technical Library
1   SATNC-AI

    Commander, U.S. Army Satellite Communications Agency, Fort Monmouth, NJ 07703
1   ATTN: Technical Document Center

    Commander, U.S. Army Tank-Automotive Command, Warren, MI 48397-5000
1   ATTN: AMSTA-ZSK
1   AMSTA-TSL, Technical Library
1   AMSTA-SF

    President, Airborne, Electronics and Special Warfare Board, Fort Bragg, NC 28307
1   ATTN: Library

No. of Copies	To

Director, U.S. Army Research Laboratory, Weapons Technology, Aberdeen Proving Ground, MD 21005-5066
1 ATTN: AMSRL-WT
2   Technical Library

Commander, Dugway Proving Ground, UT 84022
1 ATTN: Technical Library, Technical Information Division

Commander, U.S. Army Research Laboratory, 2800 Powder Mill Road, Adelphi, MD 20783
1 ATTN: AMSRL-SS

Director, Benet Weapons Laboratory, LCWSL, USA AMCCOM, Watervliet, NY 12189
1 ATTN: AMSMC-LCB-TL
1   AMSMC-LCB-R
1   AMSMC-LCB-RM
1   AMSMC-LCB-RP

Commander, U.S. Army Foreign Science and Technology Center, 220 7th Street, N.E., Charlottesville, VA 22901-5396
3 ATTN: AIFRTC, Applied Technologies Branch, Gerald Schlesinger

Commander, U.S. Army Aeromedical Research Unit, P.O. Box 577, Fort Rucker, AL 36360
1 ATTN: Technical Library

U.S. Army Aviation Training Library, Fort Rucker, AL 36360
1 ATTN: Building 5906-5907

Commander, U.S. Army Agency for Aviation Safety, Fort Rucker, AL 3636
1 ATTN: Technical Library

Commander, Clarke Engineer School Library, 3202 Nebraska Ave., N., Fort Leonard Wood, MO 65473-5000
1 ATTN: Library

Commander, U.S. Army Engineer Waterways Experiment Station, P.O. Box 631, Vicksburg, MS 39180
1 ATTN: Research Center Library

Commandant, U.S. Army Quartermaster School, Fort Lee, VA 23801
1 ATTN: Quartermaster School Library

Naval Research Laboratory, Washington, DC 20375
1 ATTN: Code 6384

Chief of Naval Research, Arlington, VA 22217
1 ATTN: Code 471

Commander, U.S. Air Force Wright Research and Development Center, Wright-Patterson Air Force Base, OH 45433-6523
1 ATTN: WRDC/MLLP, M. Forney, Jr.
1   WRDC/MLBC, Mr. Stanley Schulman

No. of Copies	To
	U.S. Department of Commerce, National Institute of Standards and Technology, Gaithersburg, MD 20899
1	ATTN: Stephen M. Hsu, Chief, Ceramics Division, Institute for Materials Science and Engineering
1	Committee on Marine Structures, Marine Board, National Research Council, 2101 Constitution Avenue, N.W., Washington, DC 20418
1	Materials Sciences Corporation, Suite 250, 500 Office Center Drive, Fort Washington, PA 19034
1	Charles Stark Draper Laboratory, 555 Technology Square, Cambridge, MA 02139
	General Dynamics, Convair Aerospace Division, P.O. Box 748, Fort Worth, TX 76101
1	ATTN: Mfg. Engineering Technical Library
	Plastics Technical Evaluation Center, PLASTEC, ARDEC, Bldg. 355N, Picatinny Arsenal, NJ 07806-5000
1	ATTN: Harry Pebly
1	Department of the Army, Aerostructures Directorate, MS-266, U.S. Army Aviation R&T Activity - AVSCOM, Langley Research Center, Hampton, VA 23665-5225
1	NASA - Langley Research Center, Hampton, VA 23665-5255
	U.S. Army Vehicle Propulsion Directorate, NASA Lewis Research Center, 2100 Brookpark Road, Cleveland, OH 44135-3191
1	ATTN: AMSRL-VP
	Director, Defense Intelligence Agency, Washington, DC 20340-6053
1	ATTN: PAQ-4B (Dr. Kenneth Crelling)
	U.S. Army Communications and Electronics Command, Fort Monmouth, NJ 07703
1	ATTN: Technical Library
	U.S. Army Research Laboratory, Electronic Power Sources Directorate, Fort Monmouth, NJ 07703
1	ATTN: Technical Library
	Director, U.S. Army Research Laboratory, Watertown, MA 02172-0001
2	ATTN: AMSRL-OP-WT-IS, Technical Library
5	Author